

AUTOMATING A SEISMIC SURVEY USING HETEROGENOUS SENSOR
TEAMS AND UNMANNED AERIAL VEHICLES

A Thesis

Presented to

The Faculty of the Department of Electrical and Computer Engineering

University of Houston

In Partial Fulfillment

Of the Requirements for the Degree of

Master of Science in

Electrical Engineering

By

Srikanth Kandanuru Venkata Sudarshan

December 2016

AUTOMATING A SEISMIC SURVEY USING HETEROGENOUS SENSOR TEAMS
AND UNMANNED AERIAL VEHICLES

An Abstract

of a

Thesis

Presented to

the Faculty of the Department of Electrical and Computer Engineering

University of Houston

In Partial Fulfillment

Of the Requirements for the Degree of

Master of Science

in Electrical Engineering

by

Srikanth Kandanuru Venkata Sudarshan

December 2016

ACKNOWLEDGEMENT

I would first like to thank my thesis advisor Dr. Aaron T. Becker of Cullen college of Engineering (ECE) at University of Houston. The door to Prof. Becker's office was always open whenever I ran into a trouble spot or had a question about my research or writing. He consistently allowed this paper to be my work but steered me in the right direction whenever he thought I needed it.

I would also like to thank all the co-authors who were involved in this research project: Li Huang, An Nguyen, Victor Montano, Chang Li and Michael McClimans. Without their passionate participation and input, this study could not have been successfully conducted.

I would also like to acknowledge Dr. Robert Stewart of the Department of Atmospheric Sciences at the University of Houston for his support, and I am gratefully indebted to him for his treasured comments on this thesis.

Finally, I must express my very profound gratitude to my parents and Janani Radhakrishnan for providing me with unfailing support and continuous encouragement throughout my years of study and through the process of researching and writing this thesis. This accomplishment would not have been possible without them. Thank you.

Abstract:

Seismic imaging is the primary technique for subsurface exploration. It requires placing a large number of sensors (geophones) in a grid pattern, triggering a seismic event, and recording the propagating waves. The location of hydrocarbons is inferred from these readings. Traditional seismic surveying for hydrocarbons employs human laborers for sensor placement, lays miles of cabling, and then recovers the sensors. Often sites of resource or rescue interest may be difficult or hazardous to access. The major drawbacks of surveying with human deployment are the high costs and time, and risks to humans due to explosives and harsh climatic conditions. Thus, there is a substantial need to automate the process of seismic sensor placement and retrievals using robots. We propose an autonomous, heterogeneous sensor deployment system using UAVs to plant immobile sensors and deploy mobile sensors. Detailed analysis and comparison with traditional surveying were conducted. Hardware experiments and simulations prove the effectiveness of automation regarding cost and time. The proposed system overcame the drawbacks and displayed higher efficiency. The deployed sensors essentially became a wireless sensor network (WSN). Thus traditional batteries cannot sustain a WSN. Energy is the major impediment to the sustainability of WSNs. Most energy is consumed by (i) wireless transmissions of sensed data and (ii) long-distance multi-hop transmissions from the source sensors to the sink. This research also presents an optimal path-planning algorithm for sustaining WSNs and validates the claim with simulations. The research in the future aims at exploring methods to exploit emerging wireless power transfer technology by using UAVs to service the WSNs. These UAVs cut data transmissions from long to short distances by collecting sensed information and replenishing WSN's energy.

TABLE OF CONTENTS

ACKNOWLEDGEMENTS.....	v
ABSTRACT.....	vi
TABLE OF CONTENTS.....	vii
LIST OF FIGURES.....	x
CHAPTER 1 – INTRODUCTION.....	1
1.1 Seismic Survey.....	1
1.2 Data Transmission.....	4
CHAPTER 2 – DESIGNING PATHS.....	7
2.1 Related Work.....	7
2.2 Overview.....	7
2.3 Path Optimization Algorithm.....	10
2.3.1 Initializing Path with Hilbert Curve.....	11
2.3.2 Gradient Descent on a Path Composed of Waypoints.....	11
2.3.3 multiple-Traveling Salesman Problem (mTSP).....	14
2.4 Results.....	15
2.4.1 One UV.....	15
2.4.2 Multiple UVs.....	16
CHAPTER 3 – DRONE MOUNTED GEOPHONES.....	19
3.1 Overview and Related Work.....	19

3.1.1 Cabled Systems.....	20
3.1.2 Autonomous Nodal Systems.....	21
3.1.3 Seismic Drones.....	21
3.2 Experiments.....	22
3.2.1 Seismic Survey Comparison.....	24
3.2.2 Accuracy Autonomous Landing With Geophone Setup.....	28
3.2.3 Penetration and Angle with the Horizontal.....	30
CHAPTER 4 –HETEROGENOUS ROBOTIC TEAMS.....	33
4.1 Overview and Related Work.....	33
4.2 SeismicDarts.....	34
4.2.1 Design.....	34
4.2.2 Experiments.....	35
4.2.2.1 Drop Tests in Different Soils.....	35
4.2.2.2 Straight vs Twisted Fins.....	37
4.2.2.3 Shot Gather Comparison.....	37
4.2.3 Deploying and Retrieving SmartDarts.....	39
4.3 SeismicSpider.....	40
4.3.1 Design.....	41

4.3.2 Shot Gather Comparison.....	41
4.3.3 Deploying and Retrieving Hexapod.....	42
4.4 UAV and Deployment Unit.....	43
4.4.1 Design.....	43
4.4.2 Experiment.....	44
4.4.2.1 Autonomous drop demonstration and accuracy.....	44
4.4.2.2 Height vs. penetration depth.....	45
4.5 Comparison.....	47
4.5.1 Ballistic Deployment.....	47
4.5.2 Simulation Studies.....	49
CHAPTER 5- CONCLUSION AND FUTUREWORK.....	52
REFERENCES.....	54

LIST OF FIGURES

Figure 1. Comparing manual and robotic geophone placement.....	2
Figure 2. Heterogeneous sensor system.....	3
Figure 3. Power usage in a wireless sensor node.....	4
Figure 4. Evolution from traditional wireless sensor networks.....	6
Figure 5. Recharging footprint and a data-transfer footprint.....	9
Figure 6. K-Footprint.....	10
Figure 7. R-Footprint.....	12
Figure 8. mTSP Solver.....	15
Figure 9. One UAV Simulation.....	17
Figure10. Multiple UAV Simulation.....	17
Figure 11. Cost Function.....	18
Figure 12. Comparing seismic survey sensors.....	19
Figure 13. Prototypes.....	23
Figure 14. Seismic Survey Comparison.....	24
Figure 15. Shot Gather Comparison.....	26
Figure 16. Schematic traditional and proposed system.....	27
Figure 17. Survey comparison experimental overview.....	28

Figure 18. A shot gather plot comparison.....	29
Figure 19. Landing Error Ellipse.....	30
Figure 20. Box and whisker plots comparing the variations in depth	31
Figure 21. Box and whisker plots comparing the variations in angle.....	32
Figure 22. Components of the SeismicDart.....	34
Figure 23. Drop height vs. penetration depth in four soil types.....	36
Figure 24. Drop height vs. angle of deviation in four soil types.....	36
Figure 25. Straight vs. twisted fins comparison.....	37
Figure 26. Outdoor drop test comparison.....	38
Figure 27. Shot gather comparison of traditional geophones vs. autonomously dropped SeismicDart sensors.....	39
Figure 28. Shot gather comparison of traditional geophones vs. autonomously dropped SeismicDart sensors (picture).....	40
Figure 29. Seismic Spider.....	40
Figure 30. Shot gather comparison of traditional geophones vs. hexapod sensor(graph).....	42
Figure 31. Shot gather comparison of traditional geophones vs. hexapod sensor(picture).....	43
Figure 32. Deployment mechanism design.....	44

Figure 33. SmartDart accuracy test.....	46
Figure 34. Landing location of Darts.....	47
Figure 35. Pneumatic Launcher.....	48
Figure 36. Sensor surveying simulations.....	49
Figure 37. Simulation Comparision.....	49
Figure 38. Number of UAVs vs time simulation.....	50
Figure 39. Survey time for different sensor ratios.....	51

CHAPTER 1 – INTRODUCTION

1.1 Seismic Survey

Hydrocarbons (coal, oil, natural gas) supplied more than 66% of the total energy consumed according to an estimate by IEA (International Energy Agency) in 2014 [1]. The global exploration and production were recorded to be 700 billion USD in the year 2014. Avoiding hazards and maintaining safety during exploration is necessary because hydrocarbons are flammable. Remote locations often require seismic surveying, with concomitant problems of inaccessibility, harsh conditions, and transportation of bulky cables and sensors. These factors increase the cost. Traditional exploration involves planting geophones (sensors) into the soil and detecting seismic disturbances caused by vibrating trucks or dynamite detonations which act as a vibration source. As these vibrations propagate, they are reflected and refracted by different layers below the surface. Geophones sense these vibrations and store the data on board or send it to a data processing unit. The data obtained describes the amplitude of the seismic waves at the geophone locations. Instead of randomly searching for hydrocarbons, explorations are carried out using elaborate technical procedures, equipment, and skilled labor over a large area. Seismic survey increases the possibility of discovering hydrocarbon reserves in an optimal fashion, using the data obtained. Cables are used to connect the seismic recorder and the sensors, but cabling cost is proportional to area, and certain terrains are inaccessible, such as jungles or wetlands. The exploration process involves repeated manual deployment and redeployment of sensors. Applying current advancements in robotics and automation could reduce the cost, decrease time and increase precision in sensing seismic waves.

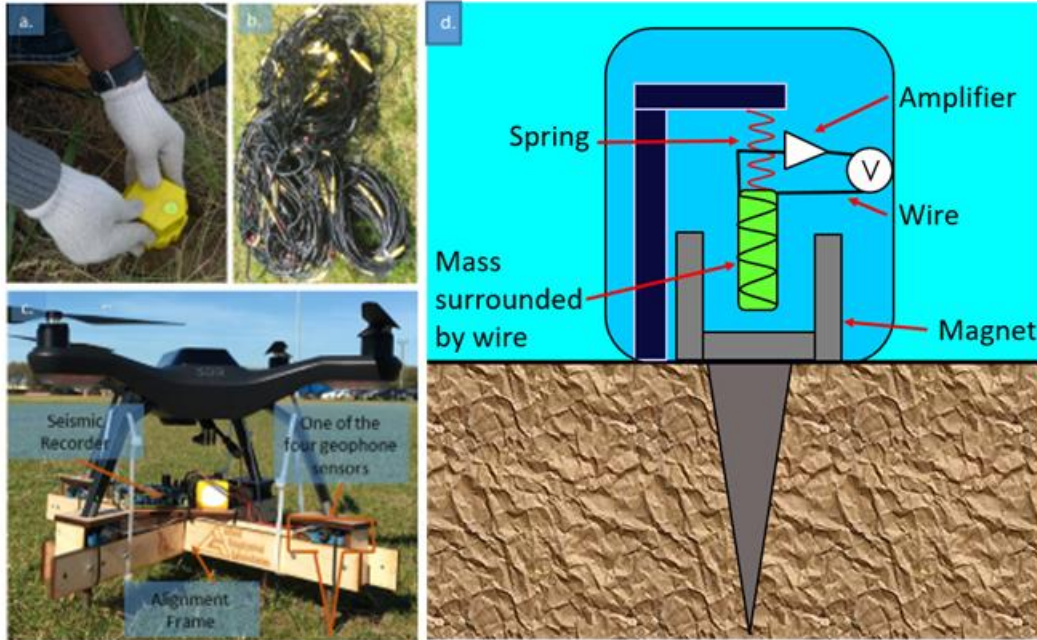


Fig. 1: Manual geophone placement. a.) Geophones are planted manually. b.) Cables for connection c.) The SeismicDrone system. d.) Geophone cross-section.

Fig. 1 displays the significant drawbacks of traditional seismic exploration. Traditional methods require cables to connect geophones to the seismic recorders and batteries and the geophone sensors are manually placed at specific locations on the field. The solution presented is a flying UAV for geophone placement and recovery. Drones or unmanned aerial vehicles (UAVs) are flying platforms with propulsion, positioning, and independent self-control.

As drone technology improves and regulations are adopted, there are major opportunities for their use in scientific measurement, engineering studies, education and agriculture. In particular, measuring mechanical vibrations is a key component of many fields, including earthquake monitoring, geotechnical engineering, and seismic surveying. Seismic imaging is one of the major techniques for subsurface exploration and involves generating a vibration which propagates into the ground, echoes, and is then recorded using

motion sensors. Numerous sites of resource or rescue interest may be difficult or hazardous to access. Also, the abundance of survey sites requires a great deal of manual labor. Thus, there is a substantial need for unmanned sensors that can be deployed by air and potentially in large numbers. The primary goal of this research is to design, build, and demonstrate the use of motion sensing drones for seismic surveys, earthquake monitoring, and remote material testing.



Fig. 2: The heterogeneous sensor system presented in this thesis, a wireless SeismicDarts and a SeismicSpider, both designed for deployment from a UAV.

We propose a heterogeneous robotic system for obtaining seismic data, shown in Fig. 2. The system consists of two types of sensors, the SeismicDart and the SeismicSpider. The SeismicDart is a dart-shaped wireless sensor that is planted in the ground when dropped from a UAV. The SeismicSpider is a mobile hexapod with three legs replaced by geophones. This system is designed to automate sensor deployment, minimizing cost and time while maximizing accuracy, repeatability, and efficiency. The technology presented

may have broad applicability where quickly deploying sensor assets is essential, including geoscience, earthquake monitoring, defense, and wildlife monitoring.

1.2 Data Transmission

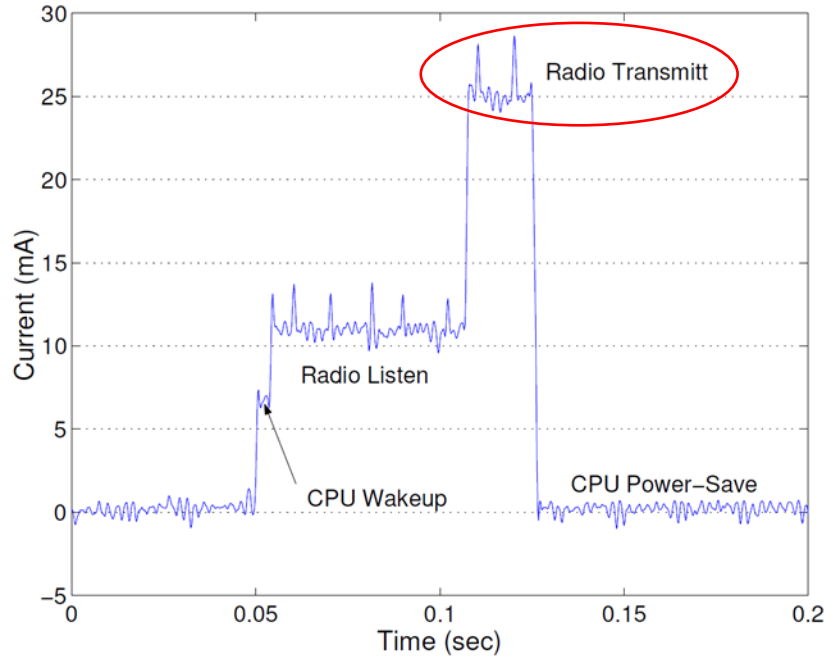


Fig. 3: Power usage in a wireless sensor node is dominated by transmission costs and listening costs. Figure modified from [2].

New wireless sensor technologies have enabled wireless sensor networks (WSNs) to proliferate in many different fields (e.g., battlefield surveillance, environmental sensing, biomedical observation [3], [4], [5], [6]). Although advances in processing and computing designs can endow sensors with a multitude of sensing modalities (temperature, pressure, light, magnetometer, infrared, etc.), advances in battery technology have been more modest. Energy constraints on battery-powered sensors limit the sustainability of WSNs. In WSNs, the majority of energy is consumed by (i) wireless transmission of perceived data [7], and (ii) long-distance multi-hop transmissions from source sensors to the sink. Radio transmission and listening dominate power usage, as shown in Fig. 3.

Harvesting environmental energy, such as solar, wind and vibration, is subject to their availability and is often uncontrollable. Incremental sensor deployment makes WSNs neither sustainable nor environmentally friendly since most disposable sensors' batteries contain cadmium, lead, mercury, copper, zinc, manganese, lithium, or potassium [8]. These heavy metals “can leach into soil and water, polluting lakes and streams, making them unfit for drinking, swimming, fishing, and supporting wildlife, and even posing hazards to human health” [9]. Fortunately, recent breakthroughs in the area of wireless power transfer technologies (e.g. inductive coupling, magnetic resonant, and RF energy harvesting) [10] provide promising alternatives for deploying such WSNs. Magnetic resonant wireless power transfer [10] can wirelessly transfer electric power from the energy storage device to the receiving device efficiently within medium range (40% efficiency within 2 meters). It is also insensitive to the neighboring environment and does not require a line of sight between the charging and receiving devices. Researchers proposed that a mobile unmanned aerial vehicle (UAV) carrying a wireless charging device could visit and recharge each sensor to sustain a WSN [11],[12].

However, one UAV may not be able to visit every sensor if the WSN is deployed in harsh environments/terrains (e.g. dense forest, mountains, underwater), or if the WSN consists of a large number of sensors. Although these seminal studies replenished sensor energy, most of the energy was still wasted by long-distance wireless transmissions of perceived data, especially by relying sensors. Due to charging and travel time of the UAV, some bottleneck sensors may drain their residual energy while waiting for the UAV. Great unsolved challenges on control remain, including how to select the optimal path for the UAV to travel within WSNs and how to efficiently dispatch multiple UAVs to recharge

WSNs. Assigning sensors to UAVs using matching theory often assumes that energy costs due to power transmission significantly exceeds the UV's transportation costs. This assumption might not fit for WSNs spread over large geographic areas, or terrain with obstacles, or where transportation costs are high, such as subsea or aerial UAVs. This research focuses on algorithms that make such WSNs sustainable by focusing on path planning, trajectory optimization and responding to dynamic network conditions, as shown in Fig. 4.

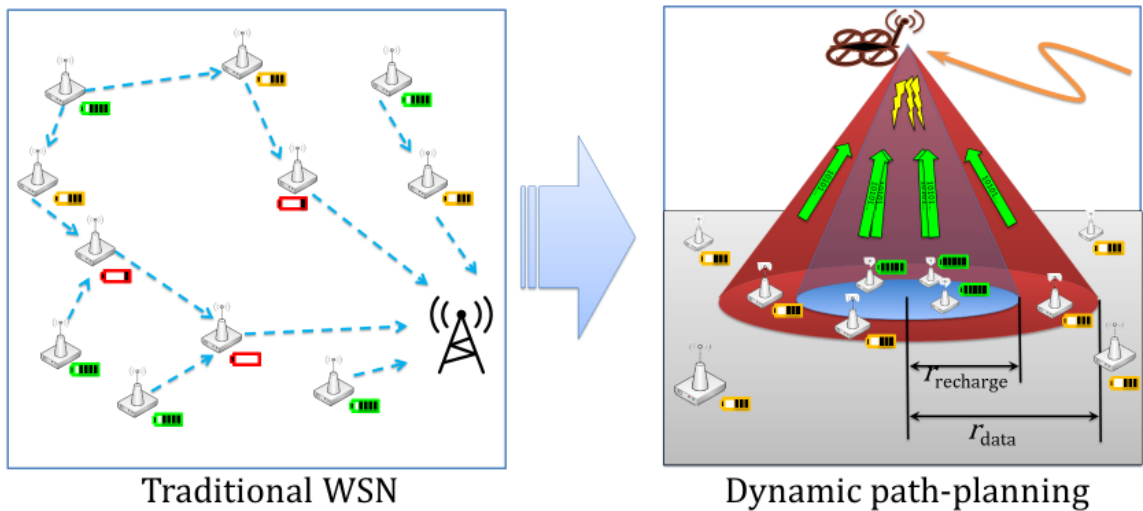


Fig. 4: Evolution of traditional WSNs to servicing WSN with UAVs. We present path planning techniques that use UAVs to gather aggregated data and recharge sensors.

Hardware components like the Raspberry Pi microcontroller and Adafruit Wi-Fi Feather boards have been used to facilitate data collection. The heterogeneous sensor teams would act as clients and upload data onto a server which is being carried by the UAV, thus reducing the energy consumed by individual sensors. Experiments have been performed to validate the data transmission.

CHAPTER 2 – DESIGNING PATHS

2.1 Related Work

The path-planning problem for UVs has been investigated from several angles. To minimize path length, the authors in [13] survey the multiple-Traveling Salesman Problem, itself a generalization of the vehicle routing problem [14]. Servicing a WSN is closely related to coverage problems recent work includes methods for optimizing speed along given routes [15], and techniques to continually improve existing routes [16]. Much work has been focused on the data ferrying problem, from minimizing the latency between visits to nodes [17], to maximizing the total data rate from sensors to sink using UVs [18], to minimizing overall delay while sharing bandwidth [19], to having a set schedule and opportunistically deviating from it [20]. Finally, using unmanned aerial vehicles to recharge other robots or sensor nodes has focused on physical design, which includes direct contact, such as swapping batteries [21], [22] or direct recharge [23], wireless resonant coupling [24], [25], and electromagnetic radiation [26], and algorithmic improvements using graph theory [27], linear programming [15], and gradient descent optimization [16].

2.2 Overview

The goal is to explore path-optimization techniques to design closed-loop paths that UVs can follow to sustain a WSN. Here sustain means a number of sensor runs out of power. Previous work often uses optimization/matching theory to assign one UV/multiple UVs to WSN nodes, and use a Hamiltonian cycle to visit each node. This is reasonable if recharging nodes is the largest component of a UV's energy budget. $E_{recharge} |nodes| \gg$

$E_{movement} \times path_length$. If this assumption is violated, path-planning becomes the key concern. A simplified form of this decision is written as

$$K_{dist} = \frac{E_{movement} \times path_length}{E_{recharge} |nodes|}. \quad (1)$$

Here K_{dist} represents the tipping point, the variable where the decision problem becomes fundamentally different. If K_{dist} is small, path-planning is inconsequential, and almost any solver is sufficient. When K_{dist} is large, path-planning becomes the key consideration. Our eventual goal is to design full trajectories that optimize the path of each UV, by servicing multiple nodes simultaneously. However, even just the path planning component is NP-hard [35]. To make progress, we focus on path optimization techniques. A UV has an associated recharging footprint and a data transfer footprint, which can often be modeled as disks of radius $r_{recharge}$ and r_{data} as illustrated in Fig. 5. If sensor nodes are clustered, a UV can service multiple clients simultaneously. We represent the fraction of sensors that are clustered as

$$K_{footprint} = \frac{2}{N^2 - N} \sum_{i=1}^N \sum_{j=i+1}^N \left(\|p_i - p_j\|_2 \leq r_{footprint} \right). \quad (2)$$

Here, p_i is the position of the i^{th} node, and there are N nodes. $K_{footprint}$ is shown in Fig. 6 for a representative network. In general, energy-efficient recharging requires closer proximity than data transmission, so this implies there are two tipping points related to node density, $K_{recharge}$, and K_{data} . Correspondingly, the WSN recharge problem has three regimes with differing solutions. Before the tipping points, nodes are sparse and not clustered. In this regime, optimal paths are straight lines from node to node, and the optimal solution is a variant of the traveling salesman problem. As sensors get closer together, the optimal path may be between one or more sensors. In Fig. 5, path A is designed to visit

each node, but path B is designed to recharge all nodes. Here, the optimal solution is often to weave between clusters of nodes. The third regime is when many nodes are close enough for transfer data, as shown in path C. The simulations in this paper take advantage of the non-zero $r_{footprint}$ to allow the UAVs to pass near sensors without requiring them to visit each node.

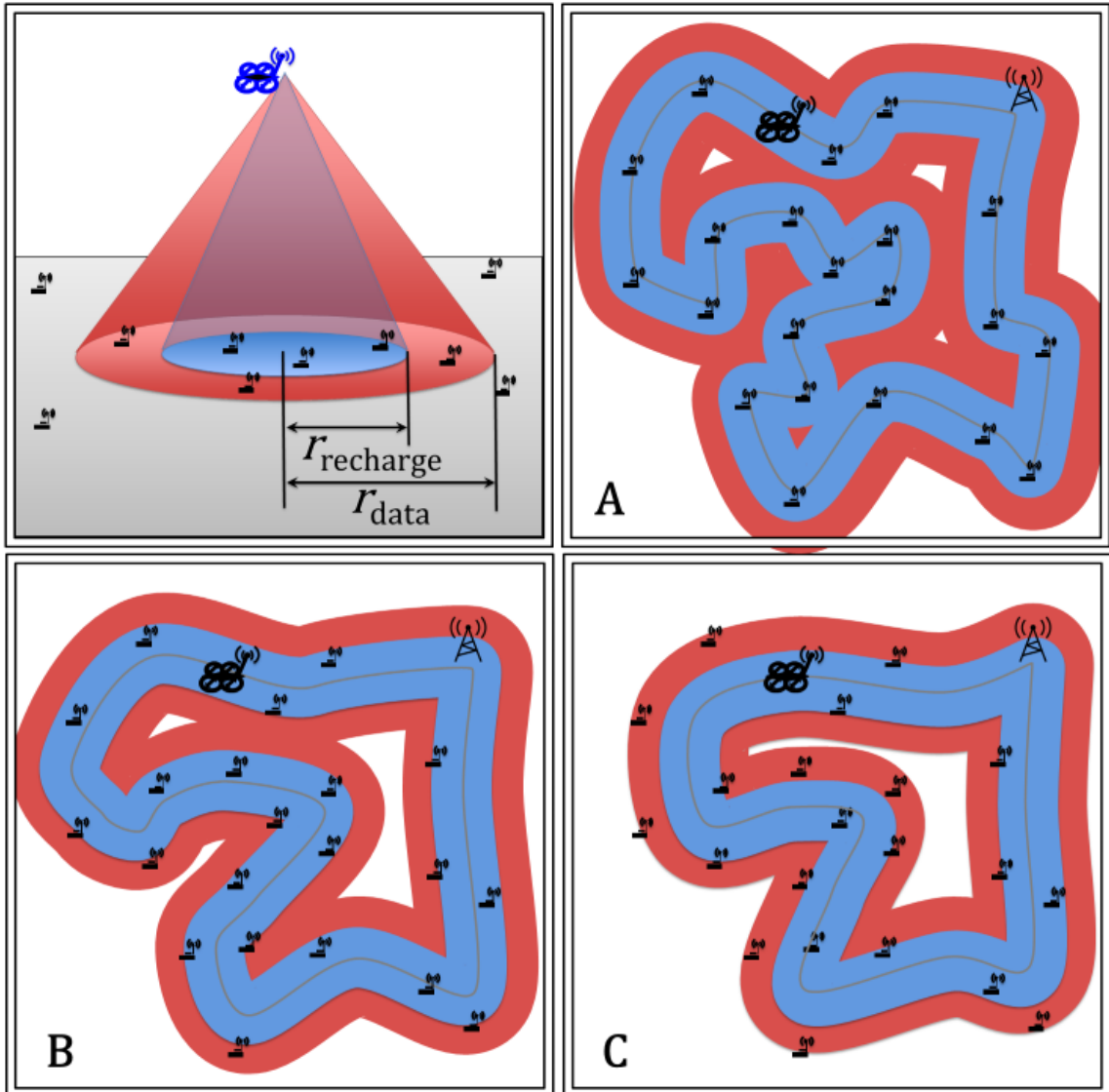


Fig. 5: A UAV has an associated recharging and data-transfer footprint. This is modeled as disks of radius $r_{recharge}$ and r_{data} . Path A visits each node, path B is designed to recharge and Path C is designed to transfer data from all nodes, and $r_{data} > r_{recharge}$.

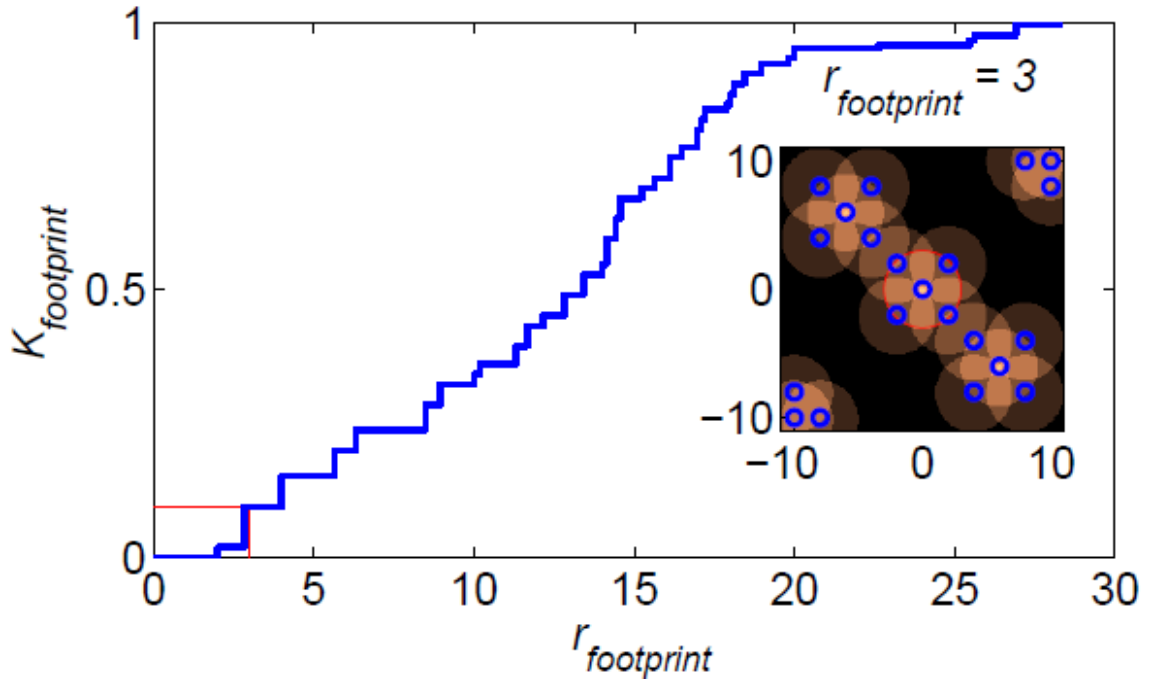


Fig. 6: As $r_{footprint}$ grows, more sensors can be recharged simultaneously. The plot above shows $K_{footprint}(r_{footprint})$, calculated by (2). The graph shows the wireless sensors (circles) and their footprints (transparent discs).

2.3 Path Optimization Algorithm

For each UV our solution designs a closed-loop path that intersects the origin. The base technique is a variant of Lloyd’s algorithm [29], [30]. Each path is represented by a finite number of waypoints, and these waypoints are both attracted to the centroid of all sensor nodes within their Voronoi cell and attracted to their neighboring waypoints. The following sections describe how this path is initialized (2.3.1), and then how the path is optimized by switching between a gradient descent optimization routine that finds local minima (2.3.2), and a genetic algorithm that rearranges the order of waypoints to improve the paths (2.3.3). Our MATLAB implementation is available at mathworks.com/matlabcentral/fileexchange/49863 [31].

2.3.1 Initializing Path with Hilbert Curve

It is important to have an initial path that fills the map. This ensures the UVs will visit every node. We adapt the space-filling Hilbert Curve, which creates a fractal path that fills up a unit area space and serves as an initial path for the first iteration [32]. The path is initialized using Hilbert's space-filling curve that is modified by connecting the start and end point to the origin making a closed loop. With multiple UVs, the Hilbert curve is scaled by a scalar to ensure the waypoints are unique.

2.3.2 Gradient Descent on a Path Composed of Waypoints

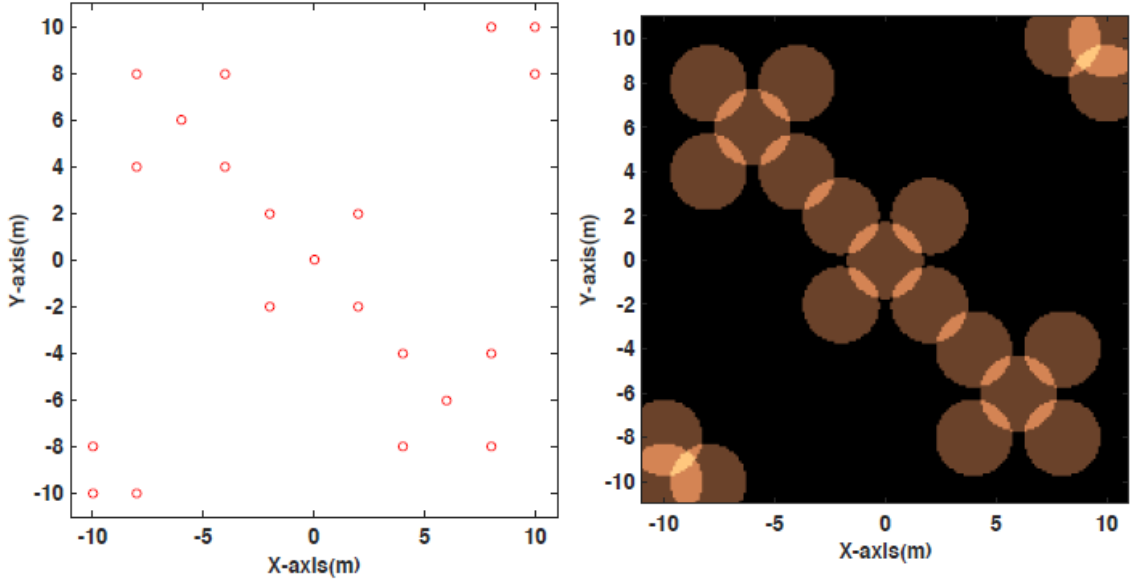
The following algorithm is derived from [31], which focused on local optimization techniques that gradually improve the paths followed by robots during persistent tasks. This technique is amenable to WSN.

Consider N UVs servicing a Wireless Sensor Network in a convex, bounded area $Q \subseteq R^2$. Waypoints are a set of points that define the path for each UV. The UV travels in a straight line in between two neighboring waypoints. Let p_i^r be the position of the i^{th} , $i \in [1, \dots, n(r)]$ waypoint of the r^{th} UV. Servicing includes recharging the nodes and collecting a part of the data that the nodes are about to transmit to the sink, thereby reducing the power expenditure in the sensor nodes. The algorithm forms a locally optimal path to visit the sensor nodes in the WSN. At each step, we compute the Voronoi partition V_i^r defined by the waypoints, with one partition assigned to each waypoint.

We require a function $\emptyset(q)$ that designates how many sensor nodes can be recharged from the position q . It tells the positions of the sensors and indicates the $r_{footprint}$ of each sensor. This information is necessary for minimizing the distance traveled by the UV and, when incorporated into the map, provides information for charging

multiple sensor nodes from a single location. For the simulation experiments, we use a binary $\phi(q)$. A simple function is used but $\phi(q)$ could also account for parameters including the maximum height at which the robot starts charging and the rate of charging to better mimic real-time performance. Here $\phi(q)$ calculates the distance between each sensor node and indicates if this distance is less than $r_{footprint}$. The reward function is given by

$$\phi(q) = \sum_{s=1}^k [(x_s - q_x)^2 + (y_s - q_y)^2] < r_{footprint}^2. \quad (3)$$



(a) Sensor node positions

(b) $\phi(\mathbf{q})$ for $r_{footprint} = 3$.

Fig. 7: Equation (3) determines the range from which a UV can service a sensor node. If $K_{footprint} > 0$, there are locations where multiple nodes can be serviced simultaneously.

In Fig. 7 (x_s, y_s) correspond to the xy location of sensor s and (q_x, q_y) correspond to the locations $q \subseteq Q$. The cost function for each path is given by,

$$H = \frac{W_s}{2} \sum_{r=1}^N \sum_{i=1}^{n(r)} \left[\int_{V_i^r} \|q - p_i^r\|^2 \phi(q) dq \right] + \frac{W_n}{2} \sum_{r=1}^N \sum_{i=1}^{n(r)} [\|p_i^r - p_{i+1}^r\|^2]. \quad (4)$$

W_s, W_n is positive scalar constants that are used to weight the sensing and neighbor distance, respectively, and depend on the experimental setup. The gradient descent algorithm minimizes the two-part cost function (4). The first part of the equation indicates a waypoint in a region far from sensor nodes is costly and the second part indicates having neighboring waypoints far away is also costly. A minimizing solution is a short path that mostly travels near WSNs.

We compute the mass, mass-moment, and centroid of the V_i^r (Voronoi partition for i^{th} waypoint of the r^{th} UV) as follows,

$$M_i^r = \int_{V_i^r} \phi(q) dq, \quad L_i^r = \int_{V_i^r} q \cdot \phi(q) dq, \quad C_i^r = \frac{L_i^r}{M_i^r}. \quad (5)$$

The control law for each waypoint is the summation of forces that pulls the waypoint toward the centroid of the Voronoi partition (weighted by $\phi(q)$),

$$u_i^r = \frac{K_i^r (M_i^r e_i^r + \alpha_i^r)}{\beta_i^r}. \quad (6)$$

Here, K_i^r is a positive definite matrix and is potentially-time varying. The first term $e_i^r = C_i^r - p_i^r$, is the error. It calculates the difference between the waypoint position p_i^r and the centroid C_i^r of the current Voronoi region. This tries to move the waypoint towards the interesting region, reshaping the path of the robot. The second term $\alpha_i^r = W_n (p_{i+1}^r + p_{i-1}^r - 2p_i^r)$ pulls the neighboring waypoints together to obtain a short path. $\beta_i^r = M_i^r + 2W_n$ normalizes the weight distribution between servicing sensors and staying close to neighboring waypoints.

The control is then applied to this waypoint to update its position,

$$p_i^r(k) = p_i^r(k-1) + u_i^r. \quad (7)$$

The control algorithm is described in Alg. 1 and is called for each waypoint in turn.

Algorithm 1 Gradient descent path optimization for the i^{th} waypoint p_i^r in robot r 's path in a known environment	
Require: Ability to calculate Voronoi partition	
Require: Knowledge of the location of neighboring waypoints p_{i-1}^r and p_{i+1}^r	
1:	loop
2:	Compute the waypoints Voronoi partition
3:	Compute C_i
4:	Obtain neighboring waypoints locations p_{i-1}^r and p_{i+1}^r
5:	Compute u_i^r
6:	Update p_i^r

2.3.3 multiple-Traveling Salesman Problem (mTSP)

The gradient descent algorithm (Alg. 1) can get stuck in local minima. To further improve the path we input the location of the waypoints obtained after running the gradient descent algorithm into a multiple-Traveling Salesman Problem (mTSP) search algorithm. Given a list of cities to visit, the classic traveling salesman problem (TSP) attempts to find an ordering of the cities that minimizes the total distance on a tour that visits all the cities once [33]. The solution is the shortest Hamilton cycle. By labeling our sensor nodes as cities, the solution to the traveling salesman problem gives the shortest length path. The mTSP solution straightens out loops in the path and can reduce the cost function. This often moves the solution out of the local minimum obtained after executing the gradient descent algorithm.

This problem is NP-hard (Non-deterministic Polynomial), but many powerful heuristics are available, and software packages can provide answers for tens of thousands of nodes (e.g., the Concorde TSP Solver [34]). A solution with multiple salesmen is called a mTSP. The mTSP is still an NP-hard problem [35], so the solutions returned by the search algorithm given limited time may not be the global optimum.

A good heuristic can increase TSP solver performance. In our numerical simulations, priming an open-source genetic algorithm solver [36] by sorting the nodes by an angle from the sink and dividing the sorted list equally between the UVs decreased path costs by 20%. Fig. 8 shows results from our simulation with 100 nodes and 5 UVs.

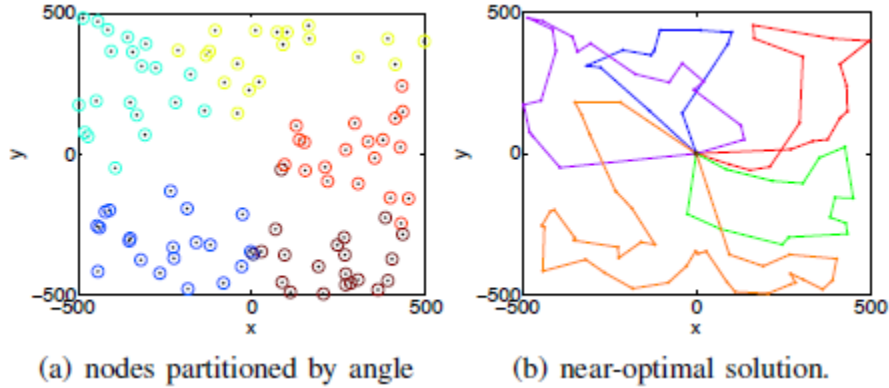


Fig. 8: Screenshots from mTSP solver aided by the heuristic. Left, nodes partitioned according to the angle from the sink. Right, the near-optimal solution from an mTSP solver aided by our heuristic.

2.4 Results

We developed a MATLAB simulation using the three algorithms described in Section 2.3. The code is available at [32]. The next two sub-sections describe the results with one UV and with multiple UVs.

2.4.1 One UV

A single UV system was simulated using MATLAB in Fig. 9. The waypoints are indicated by a set of linked ‘o’ markers, the associated Voronoi diagram is in blue, the magenta lines represent the path the UV follows for servicing the sensor nodes, and the underlying density plot represents the interesting regions generated by the sensor nodes.

The initial path at iteration 0 was set to be a space-filling Hilbert’s curve, to identify the location of the sensor nodes. If the UV follows this initial path it can learn the value function $\phi(q)$, and identify the interesting points for the whole map. A waypoint at [0, 0]

is stationary, this represents the sink where the UV recharges and unloads data collected while servicing the sensor nodes. For the first 100 iterations the gradient descent algorithm moves the path waypoints, using the Voronoi diagram to identify locations with high sensory information. The path achieved after 100 iterations, is usually a local optimum and iterating further does not decrease the cost function. This sub-optimal solution obtained often contains loops. To further optimize our path and escape this local optimum the path is inputted into an mTSP (multiple-Traveling Salesman Problem) solver for the next 100 iterations, this straightens the loops by reconnecting the waypoints without changing the waypoint location p_i^r . After 200 iterations the cost function has decreased due to the straightening of the loops by the mTSP solver. These two algorithms are repeated to optimize the cost function depending on the time available for calculation or until the cost function asymptotically converges. The cost function is shown in Fig. 11(a). This cost function monotonically decreases.

2.4.2 Multiple UVs

A two UV system was simulated on MATLAB. As shown in Fig. 10. The waypoints are indicated by green o markers, the associated Voronoi diagram is in blue, the white, cyan, magenta, and red lines represent the path the UVs follow for servicing the sensor nodes, and the underlying density plot represents the interesting regions generated by the sensor nodes.

UVs service different sets of nodes in the WSN. A multi-UV system is practical because a single UV might not be able to handle a large network. Similar to the one UV case, a space filling Hilbert's curve is used to initialize the paths. Each path contains a stationary waypoint at $[0, 0]$, representing the sink where both UVs recharge and unload

data collected while servicing the sensor nodes. The sensor nodes were placed in random locations to verify the robustness of the algorithm. The algorithm proceeds in a similar fashion to the one UV case. The simulation results in Fig. 11(b) show the optimization of the path and the minimization of the cost function.

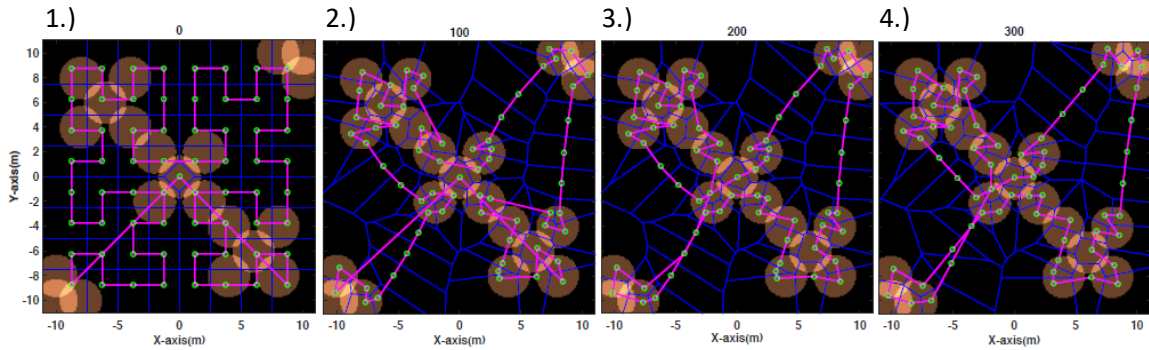


Fig. 9: Simulation for one UV. 1.) Iteration 0: Hilbert’s Space Filling Curve. 2.) Iteration 100: gradient descent algorithm (first). 3.) Iteration 200: mTSP solver (first). 4.) Iteration 300: gradient descent algorithm (second).

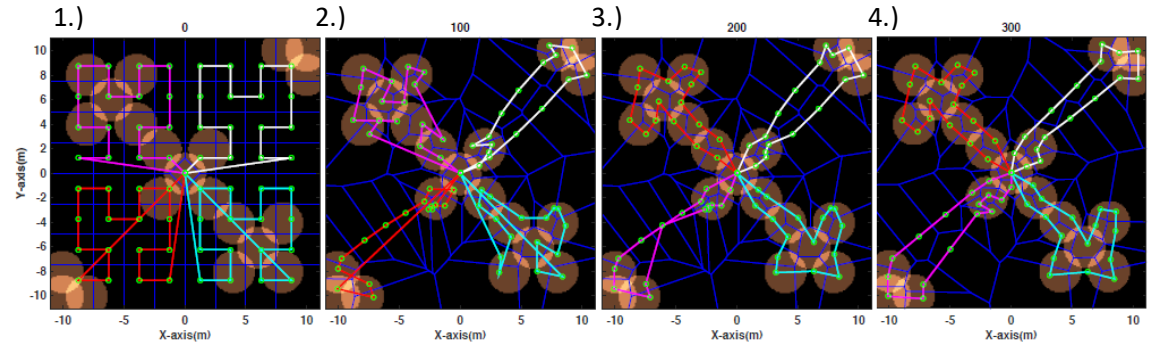
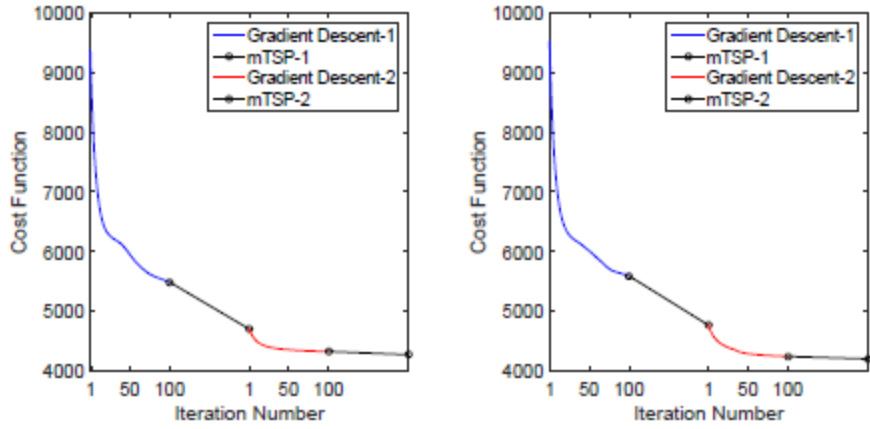


Fig.10: Simulation for multiple UVs. 1.) Iteration 0: Hilbert’s Space Filling Curve. 2.) Iteration 100: gradient descent algorithm (first). 3.) Iteration 200: mTSP solver (first). 4.) Iteration 300: gradient descent algorithm (second).



(a) Cost-function plotted for the single robot case. (b) Cost-function plotted for the four robot case.

Fig. 11: Cost function indicates a decreasing trend is approving the optimization algorithm.

CHAPTER 3 – DRONE MOUNTED GEOPHONES

3.1 Overview and Related Work

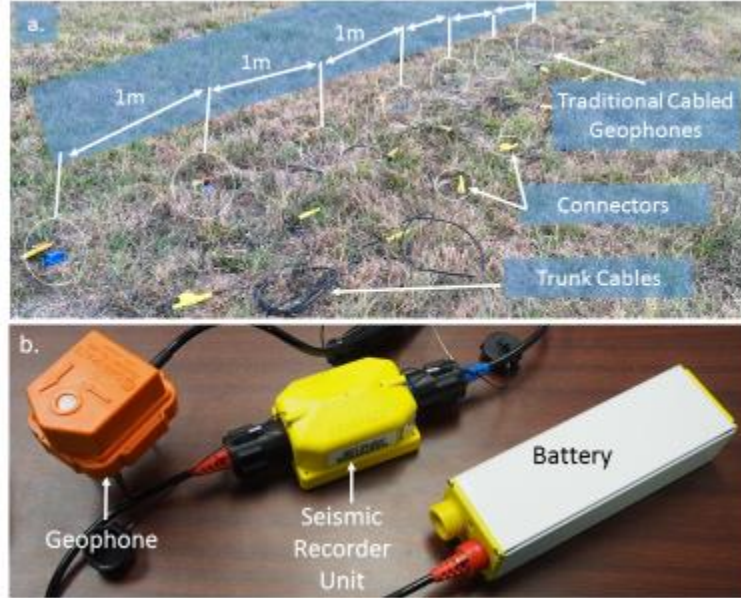


Fig. 12: Comparing state-of-the-art seismic survey sensors a.) Traditional cabled system. b.) Autonomous nodal systems.

During seismic surveys, the source of seismic/vibrational waves is excited to generate waves that propagate under the earth's surface. These waves are sensed by geophone sensors and are recorded for later analysis to detect the presence of hydrocarbons. Fig. 12 describes the current sensors available and Fig. 1c. shows the proposed solution, the seismic drone. These sensors are used to sense the vertical external displacement U caused by the vibrational waves that propagate with a velocity c in the positive and negative x -directions and is represented by the 1-D differential equation

$$\frac{\partial^2 U}{\partial t^2} = c^2 \frac{\partial^2 U}{\partial x^2}. \quad (8)$$

The velocity of a seismic wave approximately ranges from 2 - 8 km/s. Its general solution is given by

$$U(x, t) = f(x \pm ct). \quad (9)$$

The equations stated above are a generalized representation of a vibrational wave. For example, a vibrating string would satisfy the equation

$$c^2 = F/\rho. \quad (10)$$

In the above equation, c is the velocity of the wave, F is the vibration force and ρ is density. This equation is a hyperbolic equation from the theory of linear partial differential equations and is challenging to solve because of sharp features that can reflect off boundaries.

Seismic waves are detected by geophones, which detect accelerations of the earth in one dimension by enclosing a heavy magnet inside a coil of wire, movements of the magnet generate current in the coil, and are modeled as

$$m \frac{\partial^2 \varepsilon}{\partial t^2} + \mu \frac{\partial \varepsilon}{\partial t} + k\varepsilon = m \frac{\partial^2 U}{\partial x^2} - Bli. \quad (11)$$

Here ε is the coil displacement, k is the spring constant, m is the moving mass of the coil, μ is the friction coefficient, B is the magnetic flux density, l is the length of coil wire, i is the current. These equations can be found in many geophysics textbooks, for example, see [37].

3.1.1 Cabled Systems

Traditional cabled systems are extensively used for seismic data acquisition in hydrocarbon exploration. A group of sensors (geophones) is connected to each other in series using long cables, and this setup is connected to a seismic recorder and battery. The seismic recorder consists of a micro-controller which synchronizes the data acquired with a GPS signal and store the data onboard. Four cell Lithium Polymer (LiPo, 14.8V, 10Ahrs)

batteries are used to power this system. This method of data acquisition requires many manual laborers and a substantial expenditure for transporting the cables. The major difficulties faced in using cabled systems for data acquisition are (1.) Conducting a seismic survey in rugged terrains (2.) The manual labor available might be unskilled or expensive depending on the location.

3.1.2 Autonomous Nodal Systems

Currently, autonomous nodal systems [38] are extensively used for conducting seismic data acquisition surveys in the USA. Unlike traditional cabled systems, autonomous nodal systems are not connected using cables. The sensor, seismic recorder, and battery are all combined into a single package called a node that can autonomously record data as shown in Fig. 12. Even in these systems the data is stored in the on-board memory and can only be acquired after the survey is completed. This is disadvantageous since errors cannot be detected and rectified while conducting the survey. Recently, wireless autonomous nodes have been developed. These systems can transmit data wirelessly as a radio frequency in real time [39]. These systems still require manual laborers for planting the autonomous nodes at specific locations and deploying the large antennas necessary for wireless communication.

3.1.3 Seismic Drones

The concept of using robots to place seismic sensors dates to the 1980s. Mobile robots have placed seismic sensors on the moon [40]. Postel et al. proposed mobile robots for geophone placement [41]. Plans are underway for a swarm of seismic sensors for Mars exploration [42]. This paper presents a seismic drone. It combines the quality of data acquisition present in a traditional exploration method with an autonomous unmanned air

vehicle (UAV) which has high maneuverability and the capability of performing the precision landing. The first prototype consisted of a single geophone, an Arduino Uno microcontroller, an amplifier, and battery. Unfortunately, this system was not stable, and if the plant of the geophone spike failed, the drone fell on its side.

The second prototype has a seismic recorder, battery, and four geophones all embedded onto a platform that is attached to a UAV. This sensor platform with four geophones provided stability and acted as an extension of the drone's landing gear, solving the issue of tipping over during landing. These prototypes are shown in Fig. 3. By inputting a specific GPS location, the UAV can accurately deploy the seismic data acquisition system. A geophone senses ground movement (velocity) and convert it into a voltage, which is recorded with a seismic recorder. The deviation of this measured voltage from the baseline is called the seismic response and is analyzed for identifying and classifying the type of hydrocarbon present. The geophones obtain data which is processed by the seismic recorder and stored in the onboard memory. The seismic recorder is a microcontroller designed for seismic exploration applications and has a 24-bit accuracy on the ADC conversion, and sampling rates as low as half a millisecond. This device helps us obtains data comparable to commercially available seismic sensors. The drone system could successfully automate the deployment and recovery. By using a robot to perform the above task, costs and errors are reduced.

3.2 Experiments

The sensor platform of the seismic drone contains four geophones as shown in Fig. 13b. Similar to manual methods, the current seismic drone can only plant (submerge the spikes) in soft soil. On hard soil, the drone balances on 3 to 4 geophone spikes. Planting

the geophones ensure reliable coupling between the ground and sensor. To compensate for unsatisfactory coupling we use four geophones connected in series. The geophones are placed 20 - 30 cm apart, but due to the fast propagation of seismic waves, they can be considered as four collocated geophones. Hence, instead of one well-planted geophone at a particular location, we use four satisfactorily-planted geophones to obtain comparable results. In particular, the alignment platform ensures sensors are perpendicular to the ground.

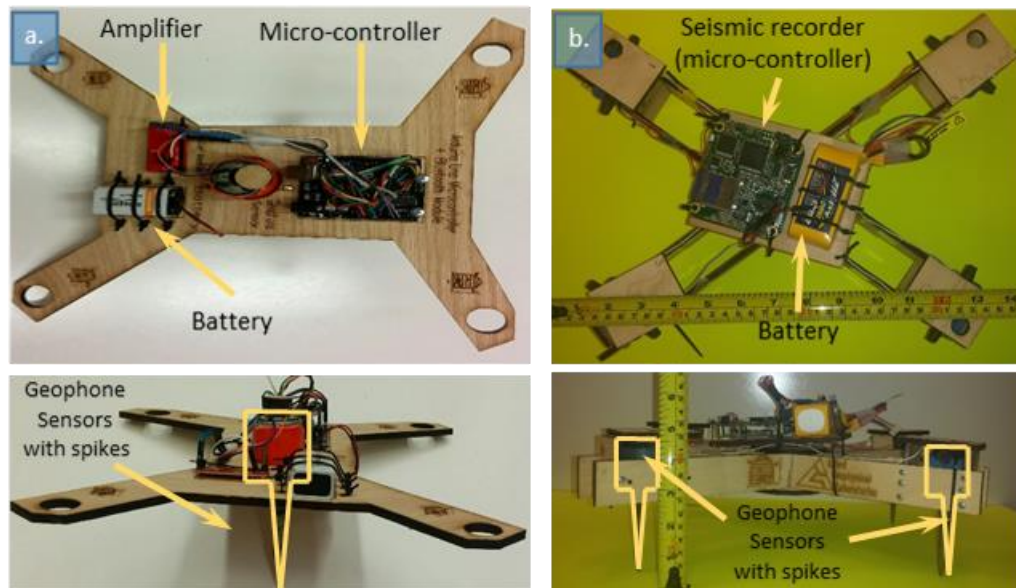


Fig. 13: a.) The first prototype consisted of a single 14Hz geophone with an Arduino Uno microcontroller and a 9V battery. b.) The second prototype consists of four 100Hz geophones, a Seismic Recorder (SR) and a LiPo battery (14.8V, 0.5Ah, 4 cells).

We conducted three experiments to prove the seismic drone is feasible. The first experiment compared sensed seismic vibrational wave output from traditional geophones and the seismic drone. This comparison validated the capability of the proposed system to replace a conventional setup. The second experiment analyzed autonomous flying with and

without the sensor platform to explore the reliability of autonomous flight and the effects of the sensor platform on the command execution capabilities due to signal interference.

The third experiment compared soil penetration and the angle of incidence in three different soil types. This is important to ensure quality data despite soil variations and shows that the platform can take off, even when the geophones are well planted in soil. Traditional geophone placement requires pushing the geophone spike into the earth to ensure ground sensor coupling. The quality of placement is determined by this coupling and the alignment of the spike with the gravity vector. Sensitivity decreases with the cosine of the angle from the spike to the gravity vector.

3.2.1 Seismic Survey Comparison



Fig. 14: Different geophone configurations are compared: a.) round platform b.) wooden platform c.) well-planted geophone d.) satisfactorily-planted geophone e.) drone system with sensor platform (Seismic Drone).

The primary experiment presented in to compare the proposed Seismic Drone performance with a traditional cabled sensing system by performing a shot gather experiment. We compare the seismic drone with different variations to understand its performance. A shot gather involves a **well-planted geophone**: a completely planted geophone where the spike is completely beneath the surface, **satisfactorily-planted geophone**: the spike is partially into the ground, a geophone mounted on a **round platform** made of fibreglass, and finally a geophone mounted on a long rectangular **wooden platform**. Each is shown in Fig. 14. Because ideal geophones are always well planted into

the ground, the platform setups and satisfactorily planted geophones were compared to show how performance varies with geophones coupling to the ground. Seismic exploration must detect the oscillating seismic wave and sensing quality is a function of coupling.

The seismic drone was flown to its respective survey location next to the well planted, satisfactorily planted, round platform and wooden platform geophones. A sledgehammer was used to strike a metal plate attached to the ground, thereby creating seismic waves for analysis.

Results show that the amplitude peaks of the seismic drone are similar to the setups (well-planted, satisfactorily-planted, round-platform, wooden-platform) as shown in Fig. 15. We observe poorly damped oscillations for the round platform and wooden platform since these are not fixed to the surface. Instead of only detecting the strike, the platform starts oscillating due to the strike and these oscillations eventually dampen out over time. The performance of the round platform, and wooden platform are poor in comparison to the well-planted geophone, which is the standard for this experiment. We observe mild oscillations in the drone setup compared to the fixed ones since these are planted into the ground. The max amplitude values are similar but do not appear simultaneously, indicating these setups were placed approximately half a meter apart, and hence a time shift occurred. The seismic drone setup and the well-planted geophone display excellent similarities in their response. This validates that the seismic drone has coupled with the surface.

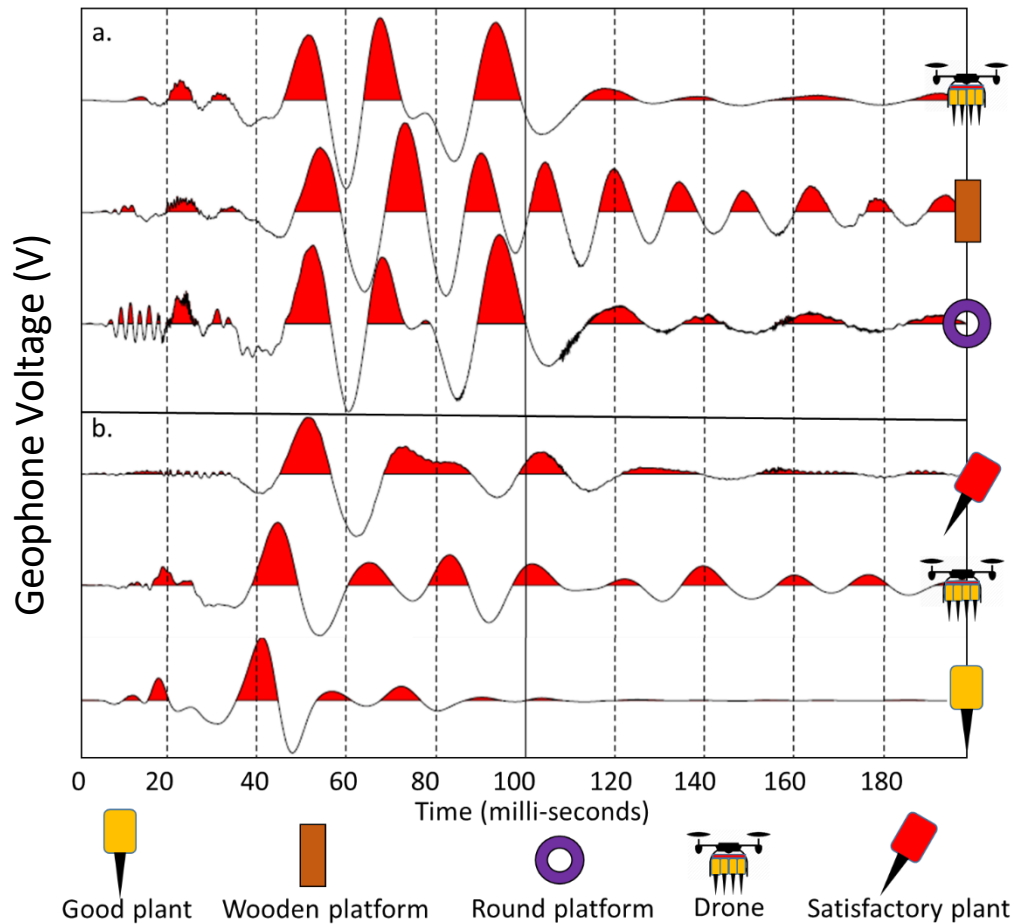


Fig. 15: Shot gather plots of the seismic wave generated by different geophone setups and the seismic drone. a.) Drone setup outperforms round and wooden platforms. b.) Compares the drone setup with well-planted and satisfactorily-planted.

Seismic explorations use thousands of geophones to conduct a seismic survey. Thus, Experiment 2 compares the performance of a traditional cabled 24 geophone system connected to a 24 channel seismic recorder and battery with an autonomous seismic drone. The geophones were planted vertically into the ground, one meter apart from one another. A schematic of the traditional setup is shown in Fig. 16 and the same experiment was repeated for the seismic drone as also shown in Fig. 16. We used a vibrating truck setup to generate the seismic wave. The geophones are well planted; the drone was flown from 1-

24 locations, and the readings were taken by generating seismic waves each time. The metal plate was struck 24 times, once for each location.

Traditional and Proposed System Comparison

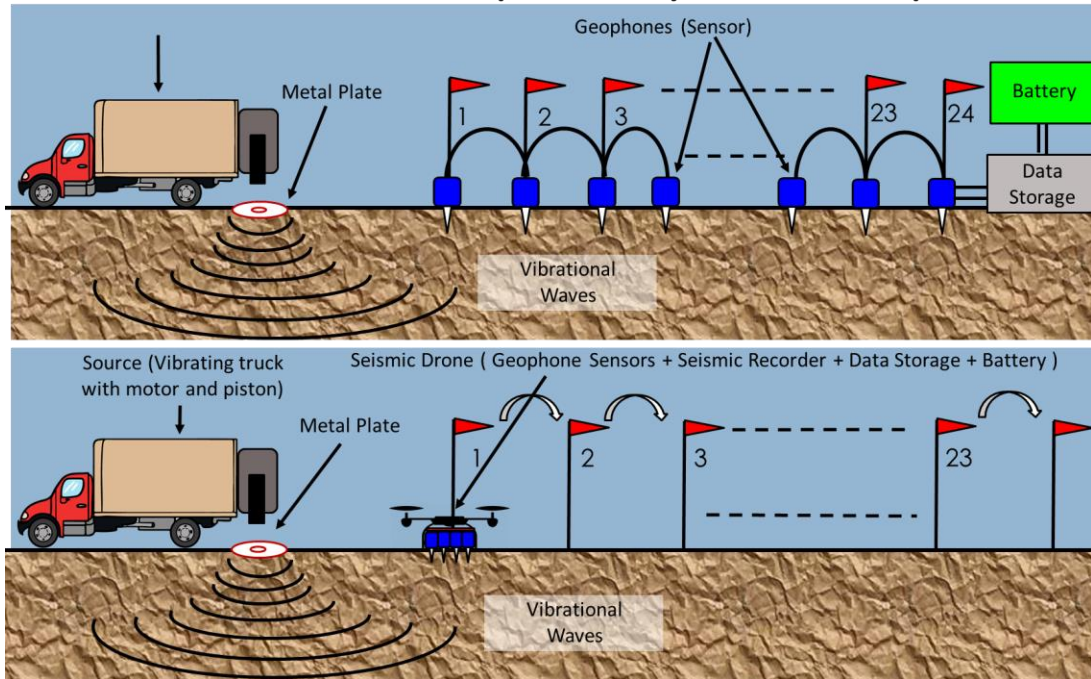


Fig. 16: A schematic of a traditional 24 geophone system, used extensively for seismic data acquisition (top). A schematic of a proposed drone setup which could replace manual laborers during seismic surveys (bottom).

Fig. 17 describes the important components of the field experiment performed. Results of the seismic survey field test comparison between a 24 channel traditional cabled geophone system and the seismic drone are shown in Fig. 18. Both plots were obtained using a Strata-Visor, a device that can obtain, store and plot the sensed data. It is extensively used with traditional geophone setups because the geophones can only sense vibrational waves and are dependent on other devices for storage and data processing. To allow a fair comparison, the autonomous setup that can store the sensed data present on the seismic drone was not used in this experiment. We observe excellent similarity, proving

the seismic drone system can compete with state-of-the-art technology in seismic exploration.

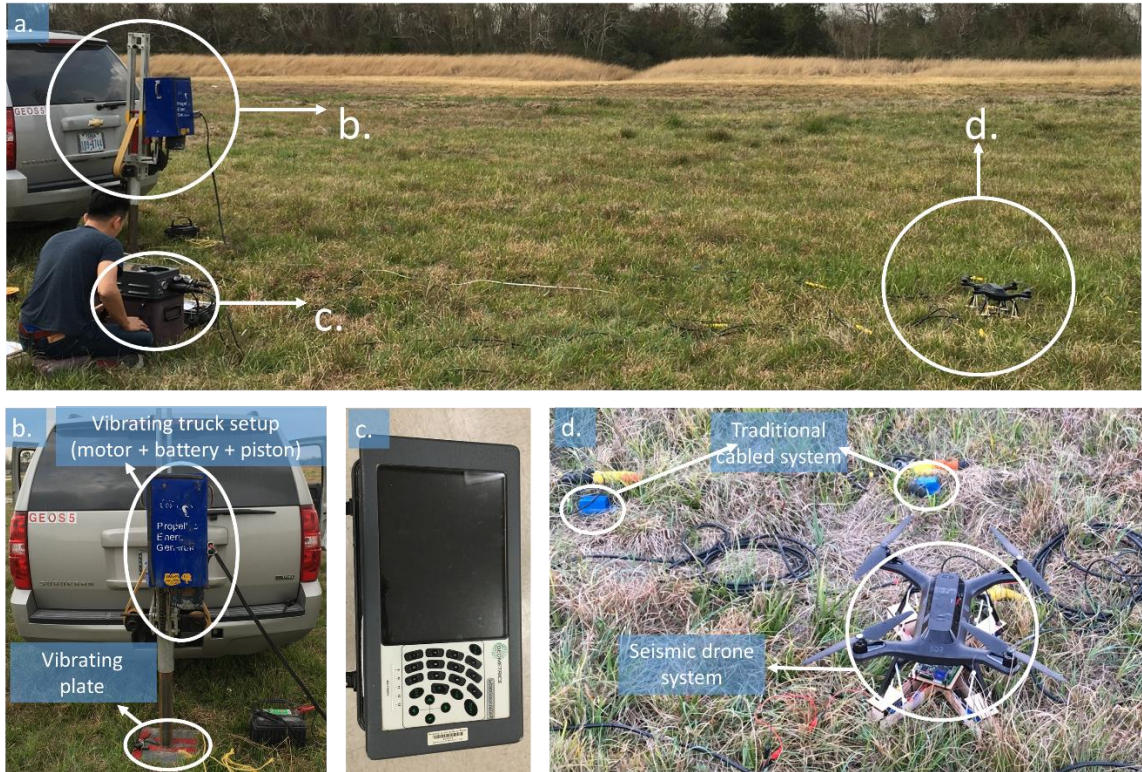


Fig. 17: a.) A survey comparison was performed to obtain the shot gather plots of the traditional cabled system and seismic drone. b.) The vibrating truck. c.) Strata-Visor. d.) The drone system and the cabled system are sensing vibrational waves.

3.2.2 Accuracy Autonomous Landing with Geophone Setup

Seismic exploration depends on the accurate placement of geophones over a large geographic area. This experiment tested the accuracy of an autonomous landing of the fully loaded seismic drone system compared to the autonomous landing of the drone system without the sensor base. The drone system used is a 3DR Solo. The seismic drone was commanded to land at the goal location marked with an 'x' using blue tape, with and without the sensor platform. The test was repeated ten times to test the accuracy of autonomous landing. The drone uses GPS for landing which is not highly accurate and hence lands at locations close to the goal location. The origin of the coordinate system was

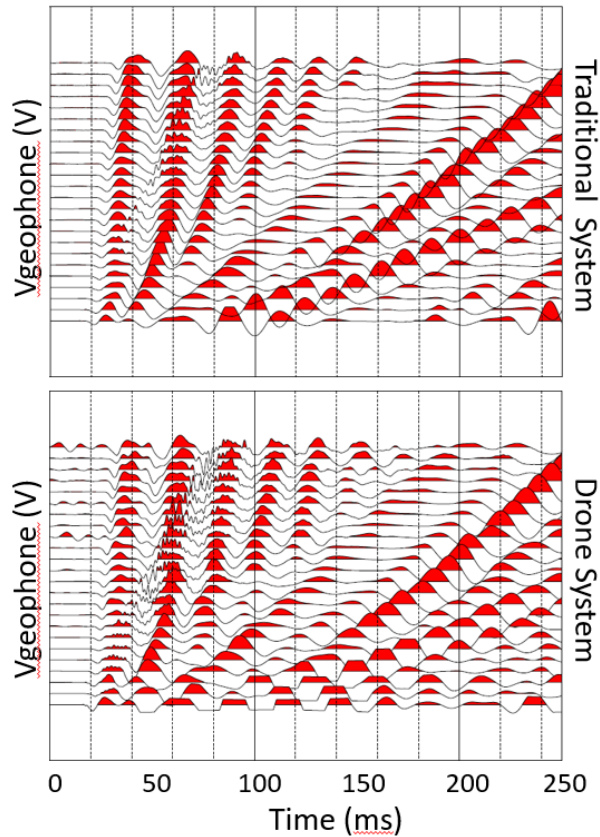


Fig. 18: A shot gather plot comparison, the x-axis is the time in milliseconds, and the y-axis is the geophone voltage. a.) Shot gather for a traditional cabled system. b.) Shot gather for the seismic drone system.

marked with an 'x' using yellow tape. Measuring tapes were used to measure landing locations. The sensor base attached to the drone for seismic sensing has four geophones. A geophone uses a strong magnet attached to spring to measure vibrations. These magnets on the sensor base influence the internal compass of the drone system with their strong magnetic fields. This effect can be observed in the plots shown in Fig. 19. The 1st and 2nd standard deviation ellipses are much smaller for the drone system without the sensor base than the system with the sensor base. The GPS used by the drone has an accuracy of five meters and landing locations are approximately normally distributed. 95% of the landings were within 1 m for the drone system without the sensor base and around 2 m for the drone

system with sensor base. The current landing accuracy is sufficient for seismic exploration because a 2 m error in distance from the landing site corresponds to an increase or decrease in travel time for the seismic wave by ≈ 25 ms.

Autonomous drone flying and landing is done using a mobile application called Tower. This app can be used to plan complex autonomous trajectories, and the drone can perform different tasks at different waypoint locations.

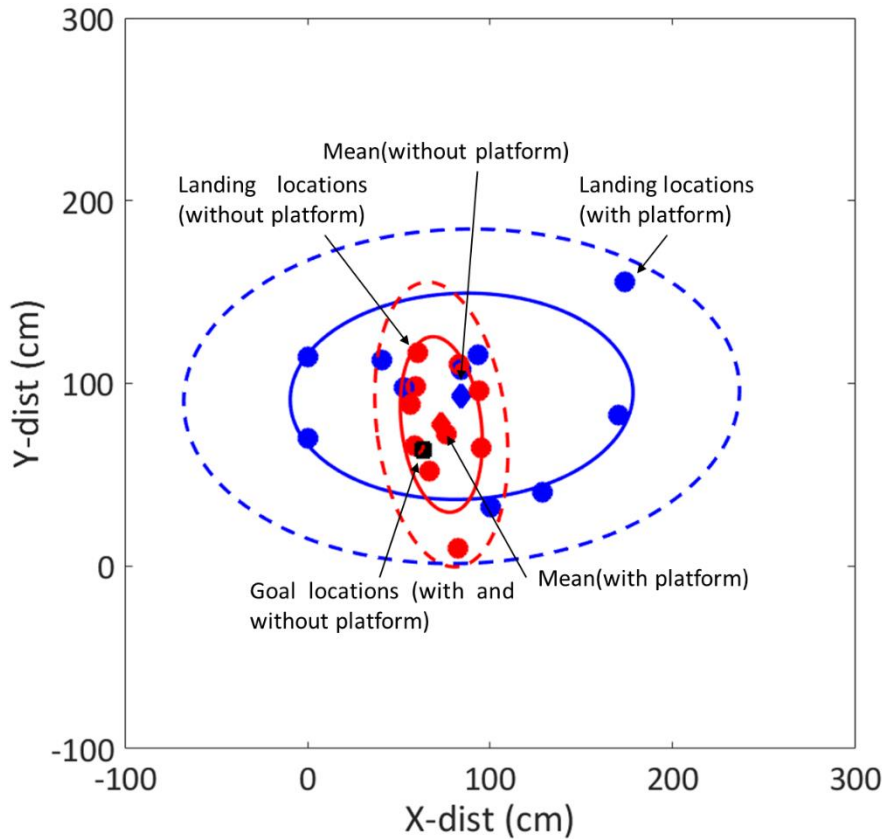


Fig. 19: The plots describe autonomous landing with and without the sensor platform for ten landings. The mean, 1st std. Ellipse and 2nd std. Ellipse are shown for both cases.

3.2.3 Penetration and Angle with the Horizontal

This experiment tests the soil penetration capabilities of the seismic drone setup in different soil types. Good coupling with soil is important for obtaining quality data. Hence

the experiment explores the penetration capability of the setup in common soils. We performed the experiment in grass, sand, and dry clay. The penetration was maximum in sand followed by grass, but the drone could not drive the geophone spike into dry clay, as shown in Fig. 20. Failing to penetrate through dry clay is inevitable even with a manual plant. Geophones are highly sensitive and can collect data without penetrating through a surface if placed vertical to the surface. Since the design considers vertical placement of geophones, a seismic analysis could be achieved by landing on any flat hard surface like dry clay, a building terrace or a road. This system could replace humans who risk lives monitoring earthquakes or perform quality checks on a partially completed bridge.

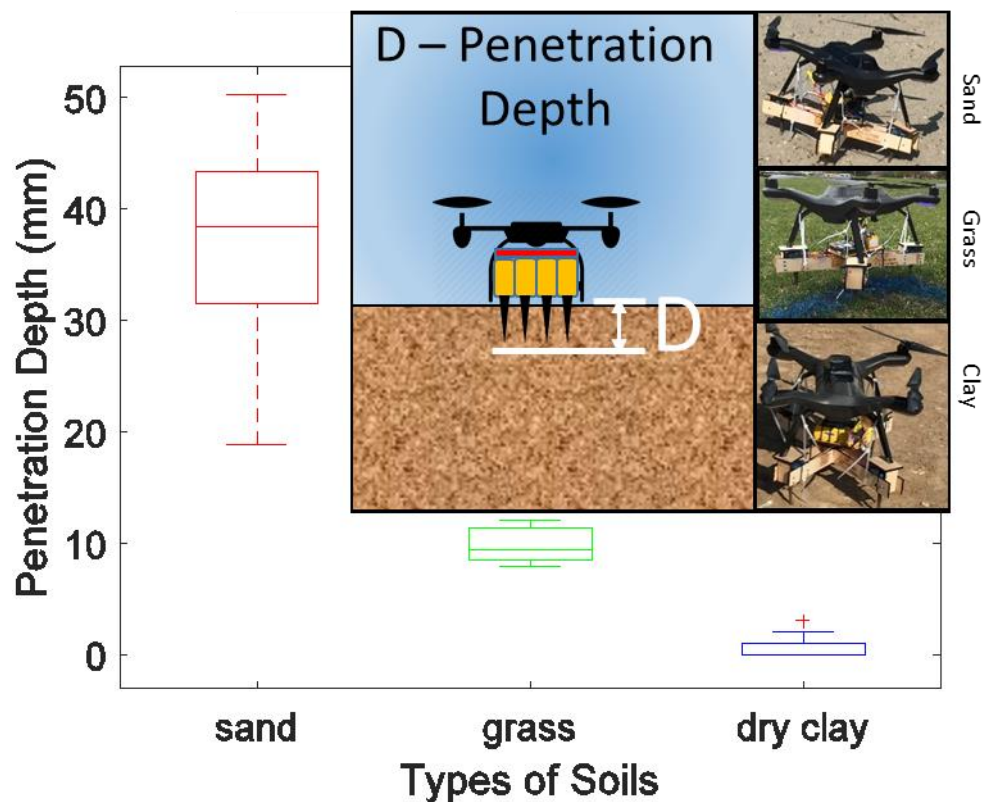


Fig. 20: Box and whisker plots comparing the variations in depth of planted geophones attached to the seismic drone.

The final experiment measured the angle of deviation of the geophone from the vertical. Ideally, geophones should be perpendicular to the ground. This is necessary to obtain quality data since the coil voltage is proportional to the cosine of this angle. A rule of thumb is to have less than 5 deg error for a geophone. It is also important to land on a flat surface with less than 10 deg deviation from vertical. The drone cannot take off if it is at an angle to the ground. These two constraints complement each other. We collected data of the roll and pitch Euler angles to calculate the deviation from the horizontal using the cross-product of rotation vectors $R_x.R_y$ (Roll.Pitch), as shown in Fig. 21.

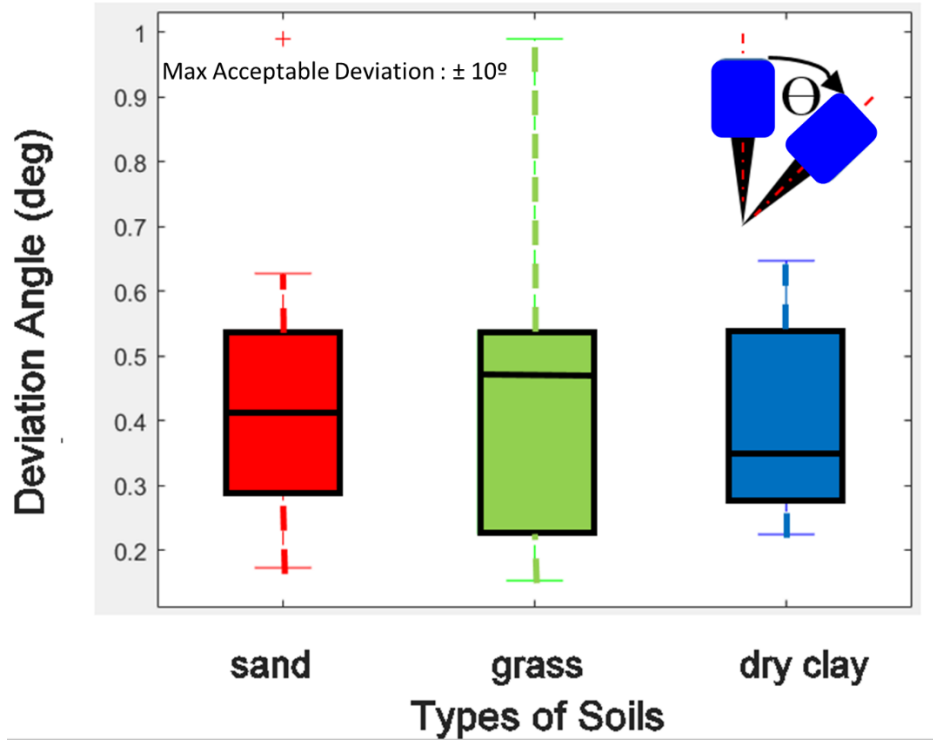


Fig. 21: Box and whisker plots comparing the variations in angle of deviation from horizontal of the seismic drone

CHAPTER 4 – HETEROGENOUS ROBOTIC TEAMS

4.1 Overview

This chapter presents a heterogeneous sensor system for automatic sensor deployment. The goal is to overcome the drawbacks of deploying seismic sensors manually. In previous work [43], we demonstrated a UAV equipped with four geophone sensors as landing gear. This UAV automated sensor deployment by flying to GPS waypoints to obtain seismic data. Magnet-coil geophones contain a permanent magnet on a spring inside a coil. The voltage across the coil is proportional to velocity. Beneath the coil, housing is a metal spike. Geophones are planted by pushing this metal spike into the ground, which improves coupling with the ground to increase sensitivity. The magnet-coil must be aligned with the gravity vector. Misalignment reduces the signal proportional to the cosine of the error.

The geophones in [43] were connected to the UAV, causing four problems: (1) one UAV was required for each additional sensor, (2) the force for planting the geophone was limited by the weight of the UAV, (3) the platform required a level landing site, (4) the magnets in the geophones distort compass readings, causing landing inaccuracy when autonomous. The proposed heterogeneous sensor system separates the sensing units from the UAV. This reduces the cost per sensor. Dropping the geophones enables increasing geophone penetration by increasing drop height and eliminates the necessity for a level landing site. The new design also increases the separation between geophones and the UAV.

Heterogeneous mobile robotic teams were used for mapping and tracking in {citehoward2006experiments}. Our system consists of a multi-agent system approach designed to quickly and efficiently perform a survey.

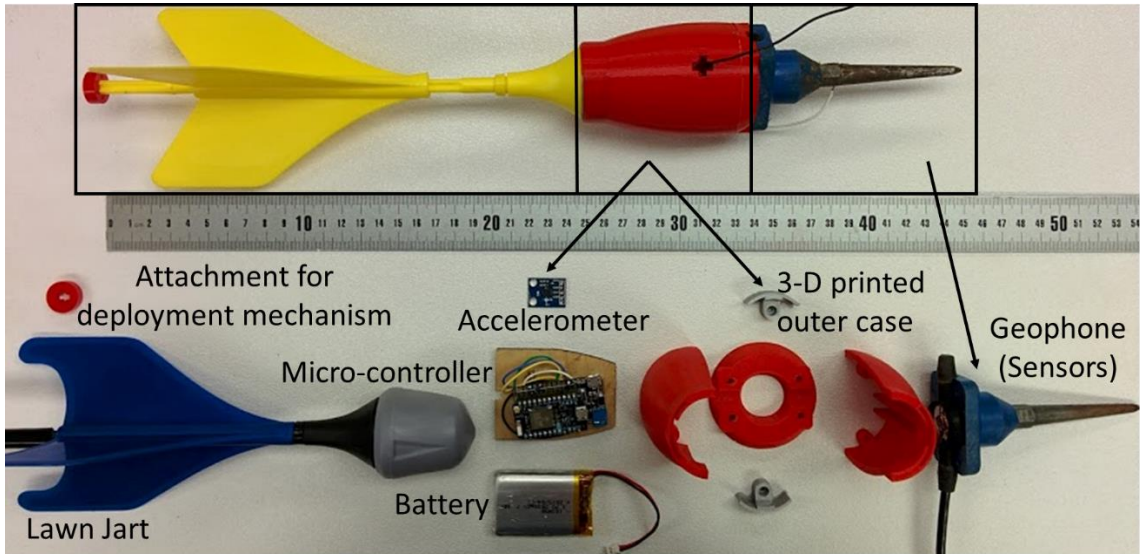


Fig. 22: Components of the SeismicDart sensor: a *Lawn Dart*TM fin, electron micro-controller, 3D printed protective casing and a geophone.

4.2 Seismic Darts

4.2.1 Design

The SeismicDart combines a geophone (GS-100) with the fins and body of a *Lawn Dart*TM, using a 3D-printed chamber that encloses a WiFi-enabled micro-controller (Electron 2G, particle.io) as shown in Fig. 22. The center of the chamber is slotted to fit a wooden plate holding an accelerometer that transmits data back to the user through the Photon. The centered accelerometer card allows placing the microcontroller and battery on opposite sides, centering the center of mass. Designs and instructions to build a SeismicDart are at [44].

4.2.2 Experiments

The following sections compare SeismicDart performance.

4.2.2.1 Drop Tests in Different Soils

This experiment varied the drop height and measured the penetration depth in four types of soil. Proper planting of a geophone requires good contact with the soil, in a vertical position. To determine the minimum height of deployment for this desired planting, each trial measured the penetration depth and angular deviation from the vertical. This experiment compared drop tests as a function of soil type.

To determine how SeismicDarts perform in different soils, this experiment measured penetration into four soil types. Each trial was performed by holding the darts at the tip opposite to the spike in a vertical position and releasing them at varying heights into the buckets of soil and measuring their penetration depth, and angular deviation. To measure penetration depth, the buried darts were marked where the spike met the soil, the dart was then pulled from the soil, and the distance from the spike tip to the marking was measured with calipers. The angular deviation was recorded from the accelerometer inside the dart. The soil types were categorized by their compression strength, in kg/cm^3 , measured using a soil pocket penetrometer (CertifiedMTP). Measurements for compression strength vary with a small deviation in measurement location, so we repeated this measurement 10 times at 10 different locations in each soil type and took the average. These values for soil compression strength and a graph displaying heights vs. penetration depth are displayed in Fig. 23, and a graph of angular deviation is in Fig. 24.

Penetrometer Readings (kg/cm^2):

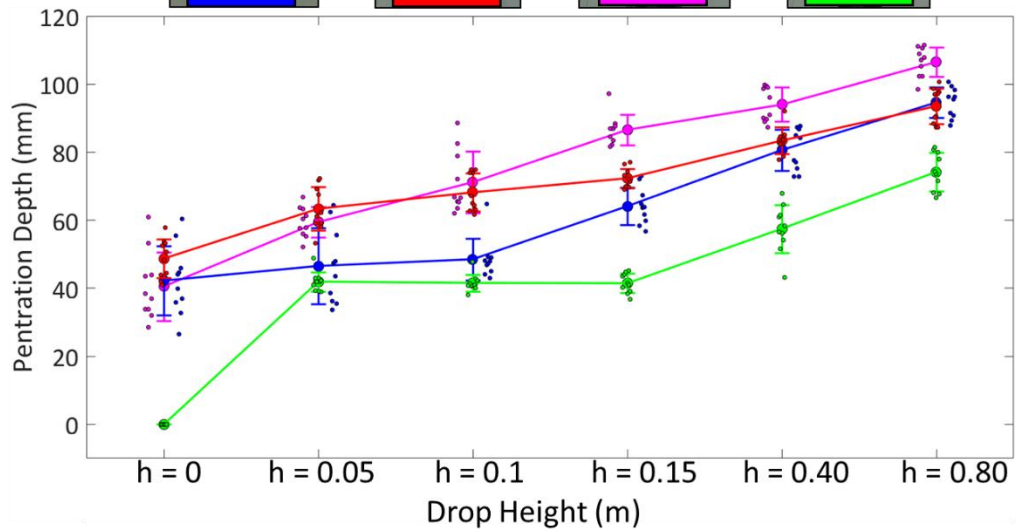
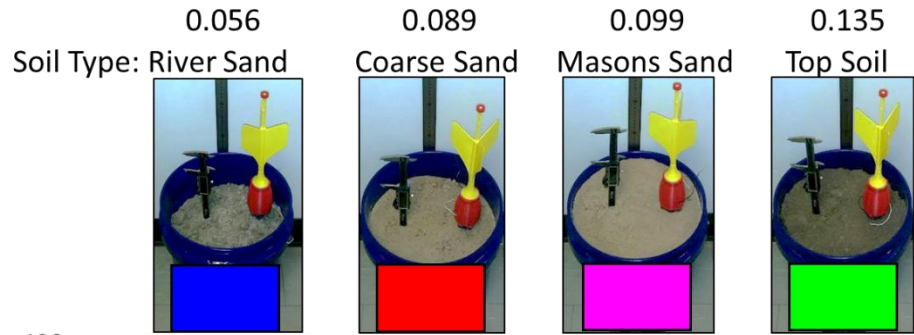


Fig. 23: Drop height vs. penetration depth in four soil types.

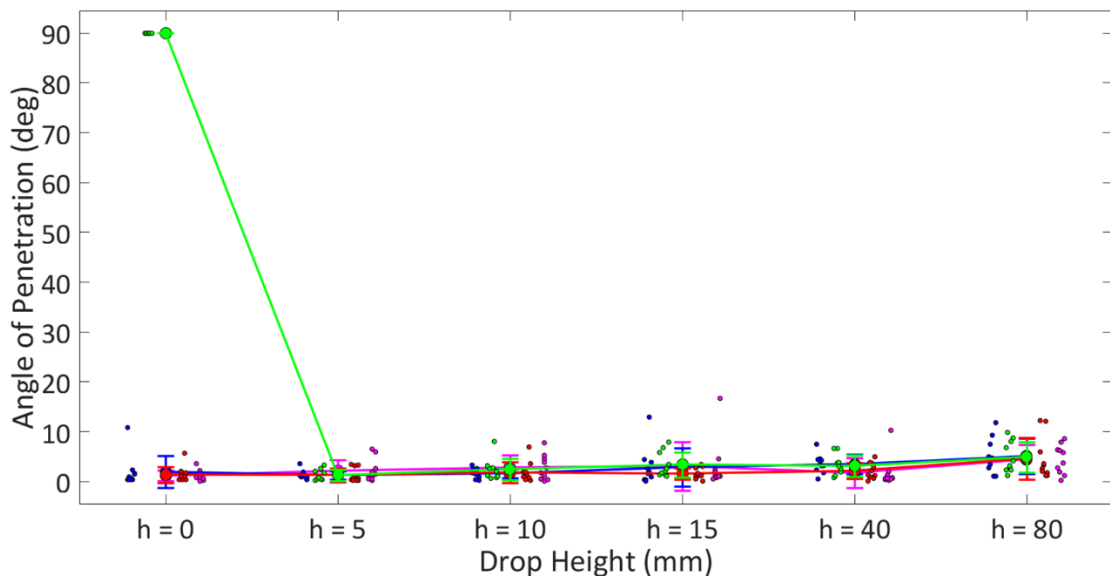


Fig. 24: Drop height vs. angle of deviation in four soil types.

4.2.2.2 Straight vs Twisted Fins

To determine the difference in performance between SeismicDarts with straight fins and twisted fins, we ran a drop test with ten trials for both types of the dart at a constant height in one soil type. As shown in Fig. 26 each trial was initialized by holding the dart horizontally at the height of 9.8 meters, dropping it into the soil, and recording the penetration depth and angular deviation. Holding the darts horizontally emphasized the angle correcting the behavior of the fins. The penetration depth and angular penetration were measured and recorded as in the other drop test experiment in different soils. A graph showing the values recorded for penetration depth and angular deviation in Fig. 25 reveals that SeismicDarts with twisted fins had a less angular deviation, but also less penetration depth.

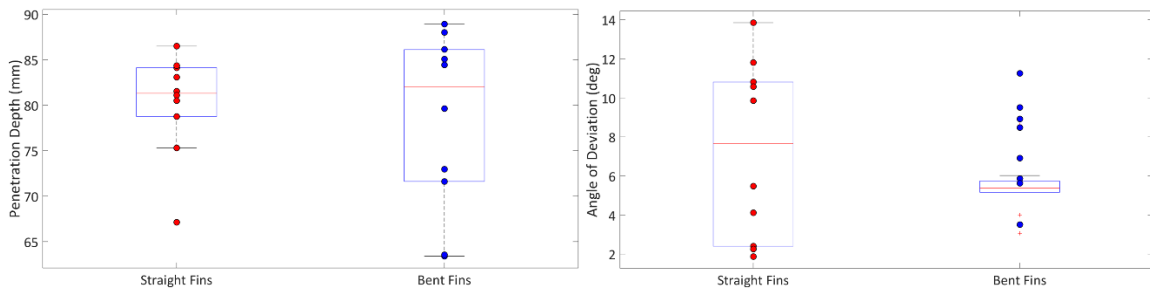


Fig. 25: Straight vs. twisted fins comparing a.) penetration depth b.) angle of deviation. The experiment used a fixed drop height of 9.8 m.

4.2.2.3 Shot Gather Comparison

Seismic explorations use thousands of geophones to conduct a seismic survey. This experiment compared the performance of a traditional cabled 24 geophone system connected to a 24 channel seismic recorder and battery with readings from SeismicDarts. The geophones were planted vertically into the ground, three meters apart from one another. We used a vibrating truck setup to generate the seismic wave. Only four functional

SeismicDarts were built, so these four were dropped from the UAV, a seismic wave was generated and recorded, and the darts were redeployed.



Fig.26: Outdoor Drop test is comparing straight vs. twisted fins performance. a.) dropping a SeismicDart b.) measuring drop height

Results of the seismic survey field test comparison between a 24 channel traditional cabled geophone system and the SeismicDarts are shown in Fig. 27. Both plots were obtained using a Strata-Visor, a device that can obtain, store and plot the sensed data. It is extensively used with traditional geophone setups because the geophones can only sense vibrational waves and are dependent on other devices for storage and data processing. To allow a fair comparison, the SeismicDart's ability to store sensed data was not used in this experiment. With the exception of SeismicDart reading #19, which may be due to poor terminal connections, the SeismicDart data corresponds well to data from a traditional setup.

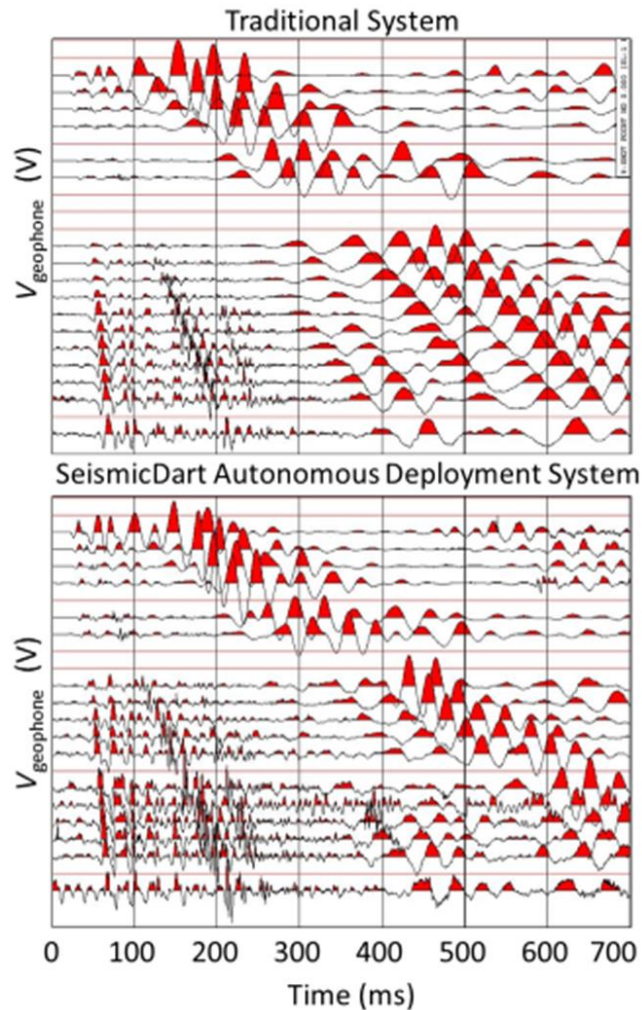


Fig. 27: Shot gather comparison of traditional geophones vs. autonomously dropped SeismicDart sensors.

4.2.3 Deploying and Retrieving SmartDarts

SeismicDarts combined with UAVs could be exploited to obtain a seismic survey quickly. Surveys of large areas require many expensive sensors. Hence deploying and retrieving are key to automating the process. Reusing sensors would drastically reduce costs. Fig. 28 shows the SeismicDart being deployed and retrieved from a location. First, the sensors (SeismicDarts) are loaded onto to UAV. Next, a flight plan is created for the deployment process. Then flight plan transfers to the UAV a set of GPS waypoint locations

that include locations where the sensor has to be dropped. Finally, the UAV flies to these locations, drops the sensors at specific location and returns home. Currently, a maximum of four sensors could be dropped in a single flight. Retrieval is currently conducted by piloting the UAV manually.



Fig. 28: Shot gather comparison of traditional geophones vs. autonomously dropped SeismicDart sensors.

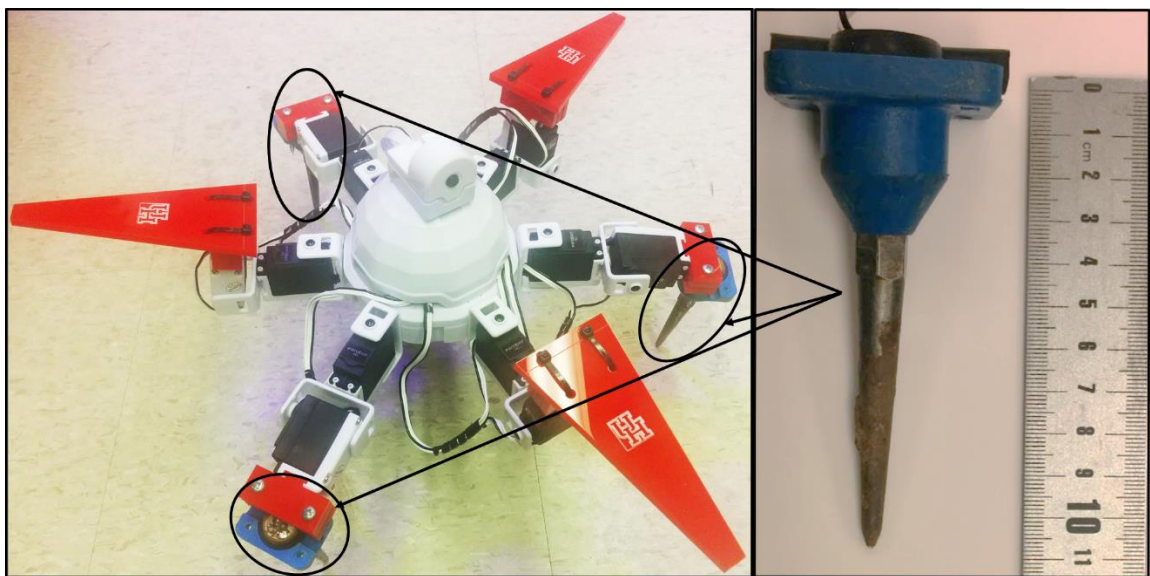


Fig. 29: The SeismicSpider is a six-legged mobile robot where three legs are replaced by geophones. It senses and records seismic data.

4.3 SeismicSpider

Traditional geophones are mounted in an insulated, shock-resistive enclosure on a spike. The spikes, varying in length, are inserted into the ground to ensure a firm coupling with the environment. The design of our SeismicSpider prevents full depth insertion of the

three-inch spikes. To overcome the coupling issue we used three geophones per robot instead of one. Our immediate goals are to compare amplitude and phase response to that of a standard single geophone.

4.3.1 Design

The Seismic Spider is built from the Six Hexapod kit designed by EZ-Robots. Each of the six legs is powered by two 15 kg/cm lever servos as shown in Fig. 29. The peg legs were replaced by three GS-20DM 14 Hz geophones from Geospace Technologies. The remaining three were designed to match the geophone dimensions and reflect UH school spirit. Our initial plan to use three geophones requires the spider to raise the three inactive legs while acquiring data. This lack of support caused excessive strain on the three servo motors responsible for holding the spider upright introducing unwanted vibration into the system. We found positioning the geophone legs at 20deg to normal enhanced the stability and relieved the excessive stress on the servos. The three geophones were in series, so with each geophone leg angled inward, superposition replicates the signal from one vertical geophone.

4.3.2 Shot Gather Comparison

A line of twenty-four geophones, GS-20DM 14 Hz, were laid out at one-meter intervals with our inline source seven meters from the nearest geophone. Beginning from the farthest offset of 31 meters, we manually aligned the Spider with the corresponding geophone, generated a vibration with the vibration truck, or sledgehammer, then moved one meter ahead.

Data from the shot gather comparison is shown in Fig. 30. We found a correlation with the standard geophones. We had to compensate for the loss of amplitude in the

traditional system since we were comparing it to the SeismicSpider which had three geophones, the response was 5 dB greater than the single geophone. The geophone wires proved insufficient to insulate against 60 Hz. Hence the raw data from the traditional setup as well as the SeismicSpider was passed through a (3-50) band-pass filter. Further, the SeismicSpider data was attenuated by -5dB to level the comparison. Due to the small amount of usable data we were not able to gain meaningful results for phase analysis.

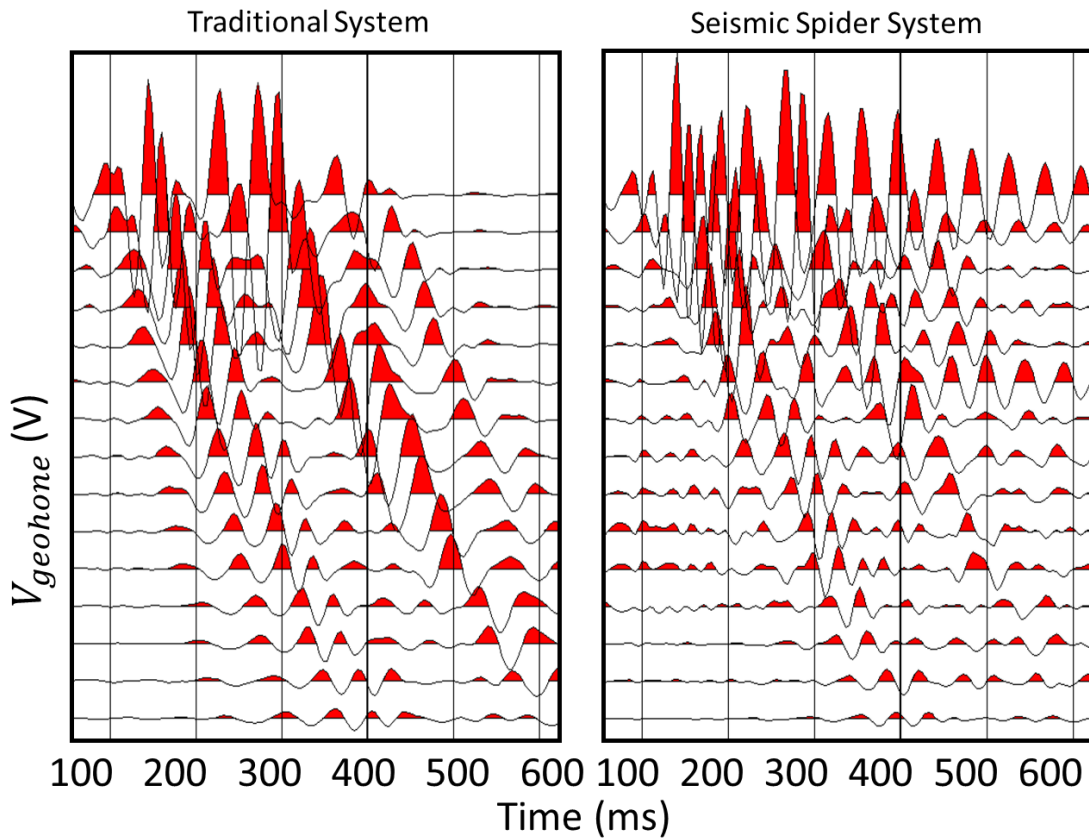


Fig. 30: Shot gather comparison of traditional geophones vs. hexapod sensor.

4.3.3 Deploying and Retrieving Hexapod

The Seismic UAV's purpose is to deploy sensors at respective GPS waypoint locations. The SeismicSpider is a mobile robot but is substantially slower compared to the

UAV. Fig. 31 shows the SeismicSpider being deployed and retrieved from a location. The UAV carrying the SeismicSpider was manually piloted to a specific location. The deployment mechanism included a hook controlled by a servo attached to the UAV. The UAV was carefully lowered, and the SeismicSpider was placed onto the ground, then the servo was triggered to unhook the sensor. The SeismicSpider was remotely activated using a mobile application. The SeismicSpider was controlled to wriggle its three standard legs to plant its three geophone legs into the ground. The SeismicSpider has an onboard GPS that could be used to navigate to a specific waypoint. Currently, autonomous deployment of sensors is possible, but the retrieval is piloted. Combining the mobility of the Seismic Spider with the speed of the UAV allows sensing at locations that are inaccessible by air or impossible to penetrate by SmartDarts.

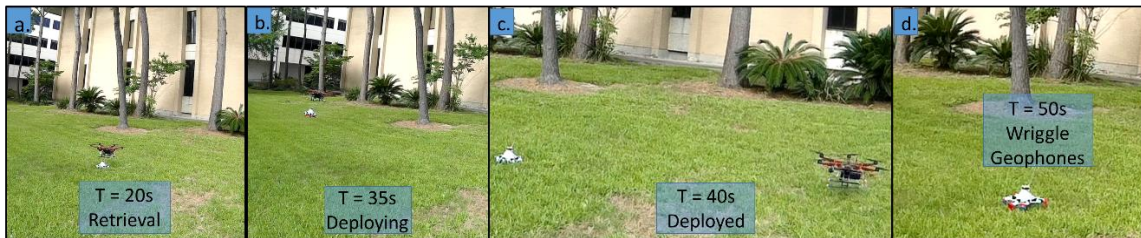


Fig. 31: Shot gather comparison of traditional geophones vs. hexapod sensor.

4.4 UAV and Deployment Unit

4.4.1 Design

The UAV is a custom-built, 177 cm wing-span hexacopter, controlled by the Pixhawk flight controller running ArduPilot Mega flight software. The UAV has a 3DR GPS module using the UBlox NEO-7 chipset. The deployment mechanism allows the UAV to carry four SeismicDarts in a circular array, and release them when it reaches the desired GPS location, one at a time, as shown in Fig. 32. The rear of the dart has a circular tip that

locks into the deployment mechanism and rests on a rectangular slot-path. A servomotor rotates the dart tips through the rectangular slot-path, allowing darts to release from a circular opening.

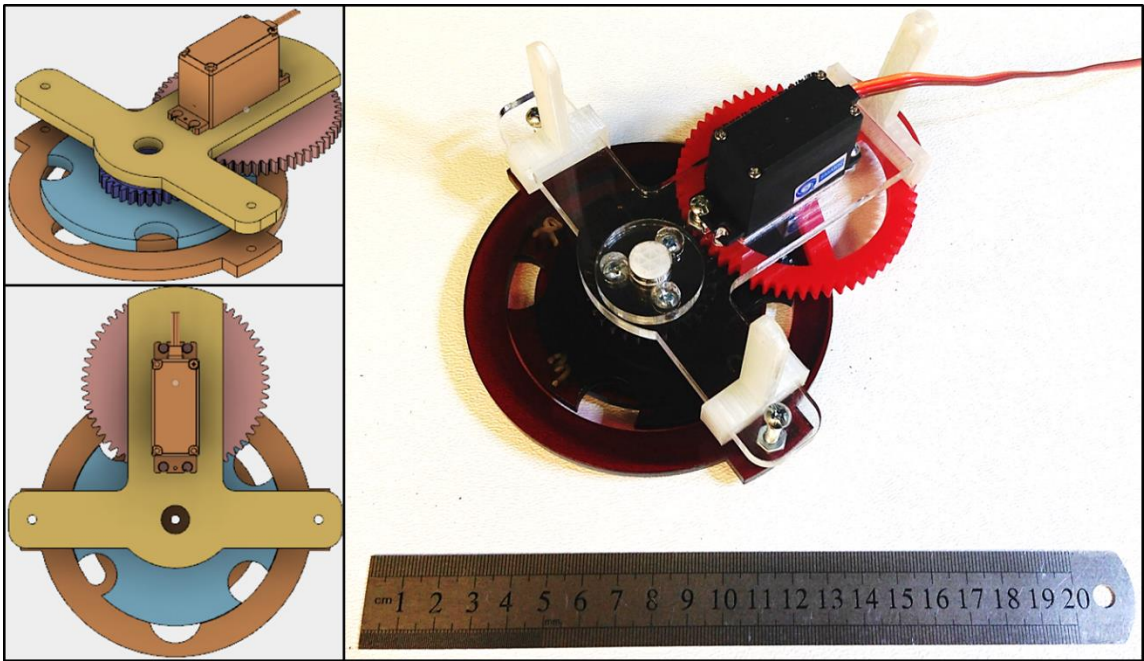


Fig. 32: Deployment system for dropping SeismicDarts from the UAV. Pictured design holds four darts, but can be scaled according to the UAV's carrying capacity.

4.4.2 Experiments

4.4.2.1 Autonomous Drop Demonstration and Accuracy

The current UAV can place the SeismicDart within ± 1 m of the desired location. This range is within tolerances for seismic surveys because: (1) often features (rocks, water, etc.) exist that require this amount of error from theoretically assigned locations, (2) some survey designs include a random placement component to improve noise cancellation, (3)

this error minimally perturbs the data since seismic waves travel at 600 m/s near the surface, so a one-meter inaccuracy equates to ≈ 1.6 ms delay.

The critical factor is to know within 10 cm accuracy the geophone location. Such accuracy can be obtained through Real Time Kinematic GPS systems. Knowledge of the exact location allows corrections for jitter in signal arrival times due to placement inaccuracy.

For the accuracy test, six sets of darts, four darts in each set, were dropped on the same GPS waypoint. To cancel out the flight controller's stable hover between each drop, the UAV traveled to a nearby GPS waypoint. This path is shown in Fig. 33a. The UAV returned to the launch platform to be reloaded, and data was recorded after each set.

To record data, one dart was picked from the first set as the reference point (the lower left in Fig. 33b), Hence the first data point will be (0,0). A 1-m T-square was placed with the origin at the dart's drop point to establish the axes.

After the first set of data had been recorded, the darts were collected and reloaded on the UAV for the next deployment set. A rod was placed in the position of the first dart to keep reference as shown in Fig. 33c. The T-square was placed and mason twine was suspended to lengthen the reference axes. Future deployments were measured using the reference point and axes. Results are shown in Fig. 34.

4.4.2.1 Height vs Penetration Depth

FAA rules require that UAVs fly below 400 feet (122 m). Our highest drop tests were from 20 m and resulted in well-planted geophones on a grass field with density 3.3 kg/cm^3 . Harder soils may require faster impact velocity, so this section examines possible impact velocities as a function of drop height. For ease of analysis, we will assume the

SeismicDart has a constant coefficient of drag C_d and that the drag force is proportional to velocity squared and equal to $\frac{1}{2} v^2 \rho A C_d$, where v is the velocity, A the cross-sectional area and ρ the density of air. The tests were performed near sea level, so $\rho \approx 1.225 \text{ kg/m}^3$, and the dart body is 0.06 m in diameter so $A = 0.028 \text{ m}^2$. We will assume the dart C_d is between that of a streamlined body $C_d = 0.04$ and that of an arrow $C_d = 1.5$ [45], and choose that of a sphere $C_d = 0.47$.

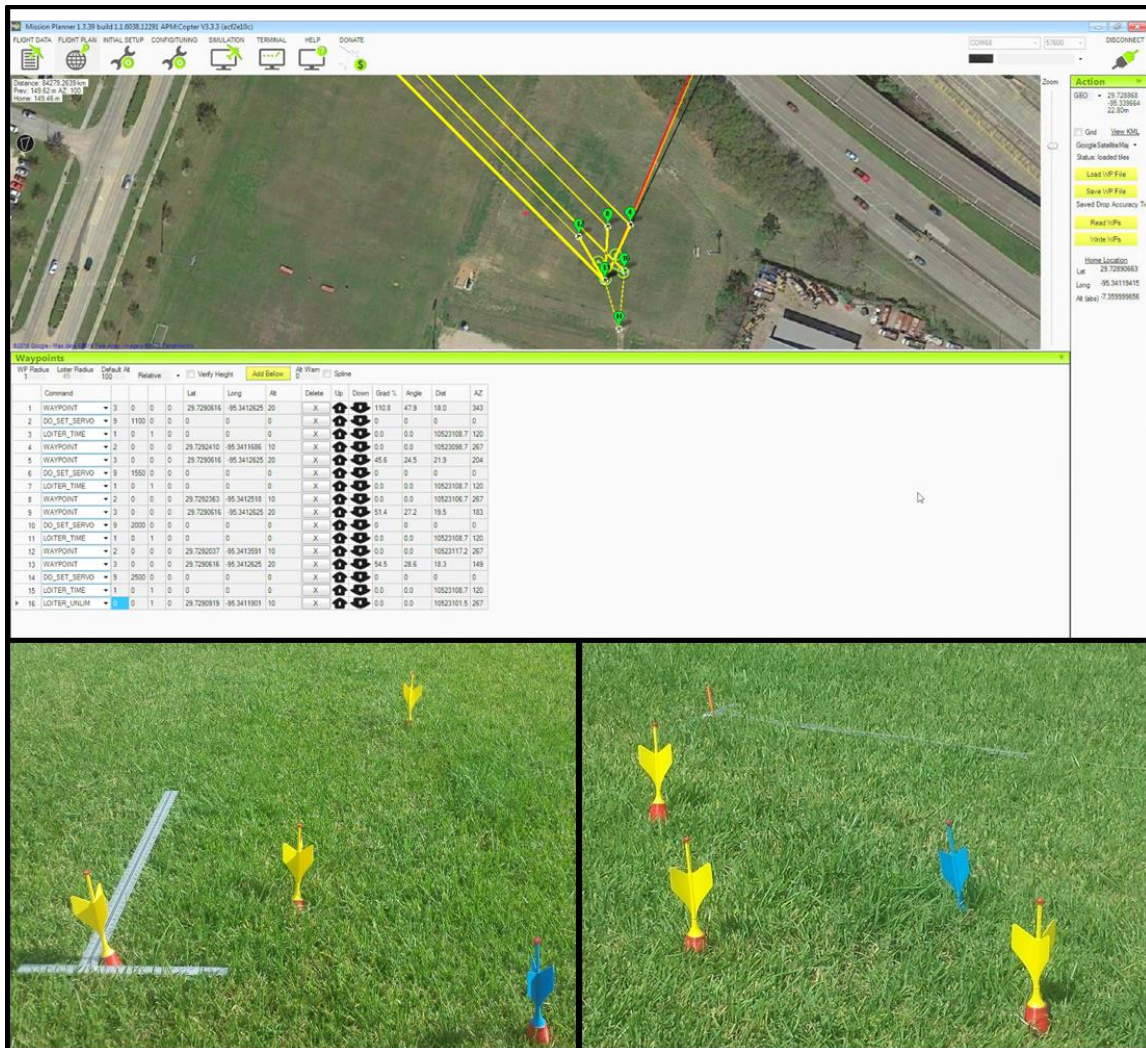


Fig. 33: a.) Flight plan of accuracy test b.) First set of the dart with reference axes c.) Third dart set

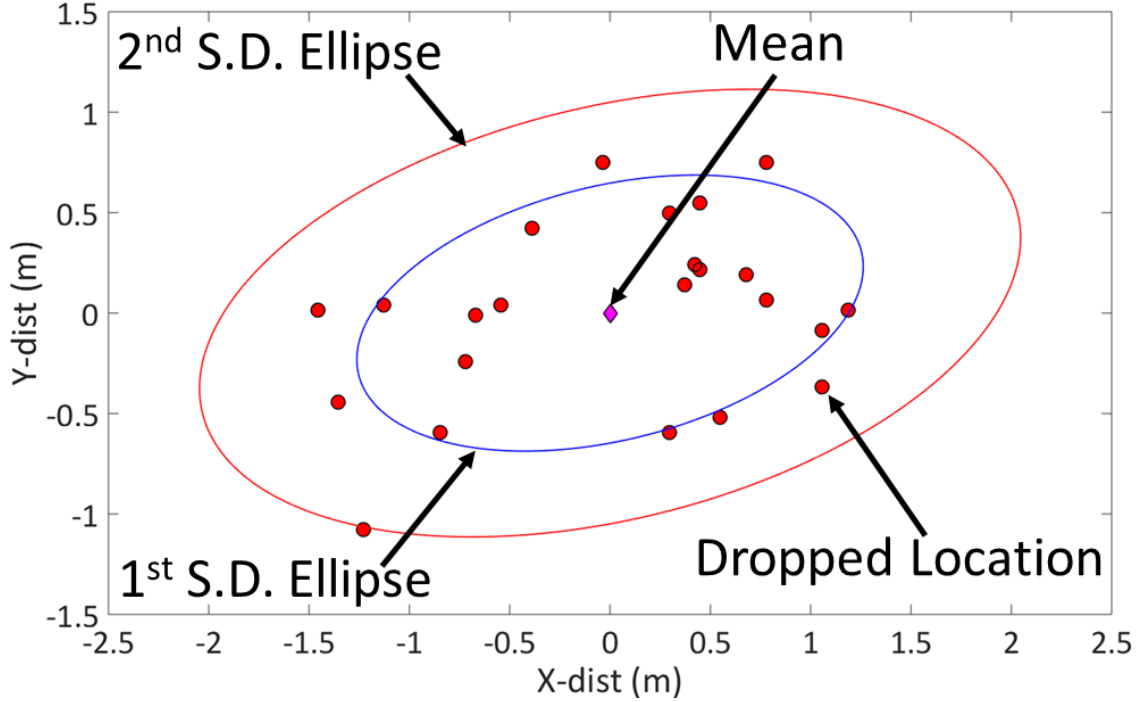


Fig. 34: Landing locations of 24 darts, each commanded to drop at the same GPS location.

The terminal velocity is

$$\vartheta\tau = \sqrt{\frac{2mg}{\rho AC_d}} \approx 59\text{m/s}. \quad (12)$$

The velocity at impact is a function of the drop height h given by

$$\vartheta_{impact} = \vartheta\tau\sqrt{1 - e^{-\frac{\rho AC_d h}{m}}} \approx 59\sqrt{1 - e^{-0.008h}}\text{m/s}. \quad (13)$$

With $C_d = 0.47$, our drop from 20m achieves only 38% the terminal velocity (19.0 m/s), and for $C_d = 0.04$ only 12% terminal velocity (19.7 m/s). This implies the SeismicDart is suitable even for much harder soils than tested this far.

4.5 Comparison

4.5.1 Ballistic Deployment

To compare an alternate deployment mechanism we built the pneumatic cannon shown in Fig. 35. The pneumatic cannon is U-shaped, 2m in length, with a 4" diameter

pressure chamber and a 3" diameter firing barrel, connected by an electronic valve (Rain Bird JTV/ASF 100). The cannon is aimed by changing the desired firing angle θ_f and azimuth angle, and filling the pressure chamber to the desired pressure. The reachable workspace is an annular ring whose radius r is a function of the firing angle and initial velocity ϑ . Neglecting air resistance, this range is found by integration

$$r = \frac{\vartheta^2}{g} \sin(2\theta_f). \quad (14)$$

Initial velocity is limited by the maximum pressure and size of the pressure chamber. The cannon used SCH 40 PVC, which is limited to a maximum pressure of 450 psi.

We charged our system to 150 psi and achieved a range of $\approx 150\text{m}$. This is considerably smaller than the UAVs range, which when loaded can complete a round trip of $\approx 1.5\text{ km}$. A larger problem illustrated in Fig. 35, is that angle of incidence θ_i is equal to the firing angle θ_f . Maximum range is achieved with $\theta_f = 45\text{deg}$, but this angle of incidence reduces the geophone sensitivity to $\cos(\theta_f) \approx 0.7$. The placement accuracy of the cannon is lower than the UAV because a fired dart must fly over a longer distance than a dropped dart. Safety reasons also limit applications for a pneumatic launcher.

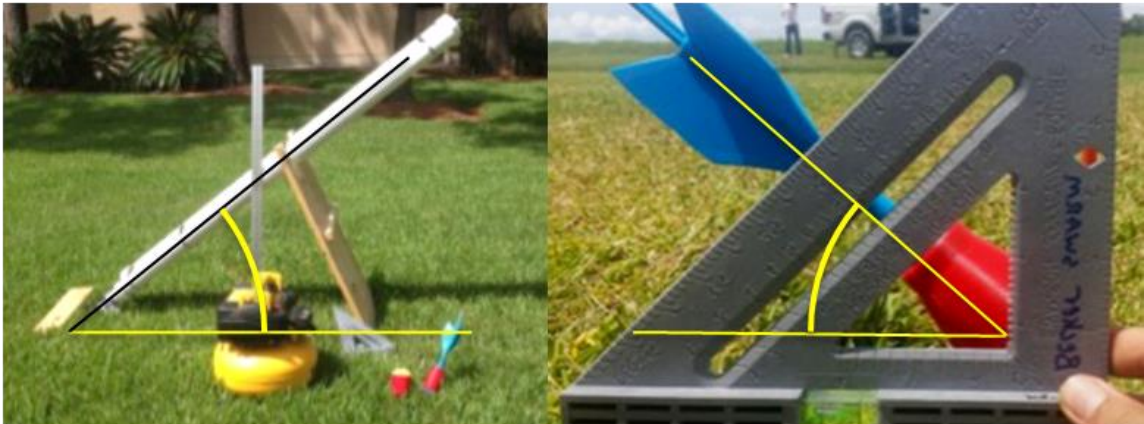


Fig. 35: A pneumatic launcher for SeismicDarts. Ballistic dart deployment has limited usefulness because the incident angle is equal to the firing angle.

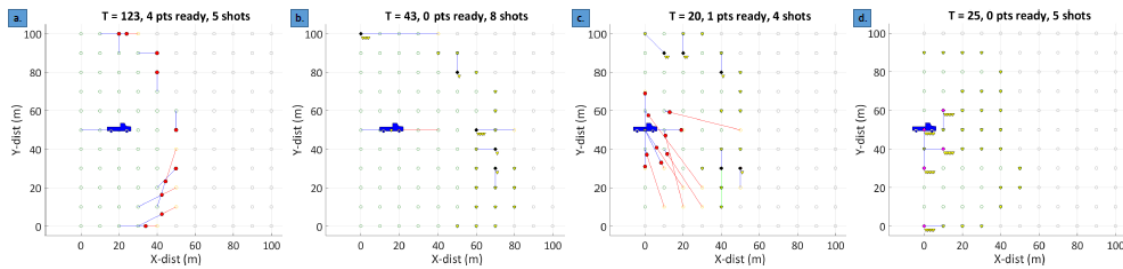


Fig. 36: Screenshots of simulations that were performed to estimate time take by different sensors surveying 100x100 m grid a.) Only SeismicSpiders b.) SeismicDarts and deployment system c.) Heterogeneous System d.) Human workers

Test	Type	Numbers of Units	Survey Time (s)	Velocity (m/s)
1.	SeismicSpiders	5000 SeismicSpiders	73,893	0.2
2.	UAVs, SeismicDarts	500 UAVs, 5000 SeismicDarts	1,216	20
3.	Workers	500 Workers, 5000 Sensors	7,371	1.38

Fig. 37: Comparison of different modes of deployment highlight the efficiency of UAV deployment.

4.5.2 Simulation Studies

A scheduling system to compare time and costs for seismic surveys with varying numbers of UAVs, SeismicSpiders, SeismicDarts, and Human manual laborers was coded in MATLAB, available at [46]. Screenshots of the different cases are shown in Fig. 36. This tool allows us to examine engineering and logistic trade-offs quickly in the simulation. For example, Fig. 38 assumes a fixed number of darts and examines the finishing time with 5 to 500 UAVs. The time required decays asymptotically, but 140 UAVs requires only twice the amount of time required for 500 UAVs, indicating that 140 UAVs are sufficient for the task. Substantial cost savings can be obtained by selecting the number of UAVs required to complete within a certain percentage greater than the optimal time.

The tool is useful for comparing the effectiveness of heterogeneous teams. Table Fig. 37 compares surveying a 1 km x 10 km strip of land with team (a) 5000 SeismicSpiders, (b) 500 UAVs and 5000 SeismicDarts, (c) 500 humans and 5000 sensors (geophones). Team (b) completed six times faster than the team (c). The SeismicSpiders are much slower even compared to humans, but these sensors are useful during special cases. Since the SeismicSpiders are 100x slower than the UAVs and expensive compared to the SeismicDarts, their use could be limited to special occasions.

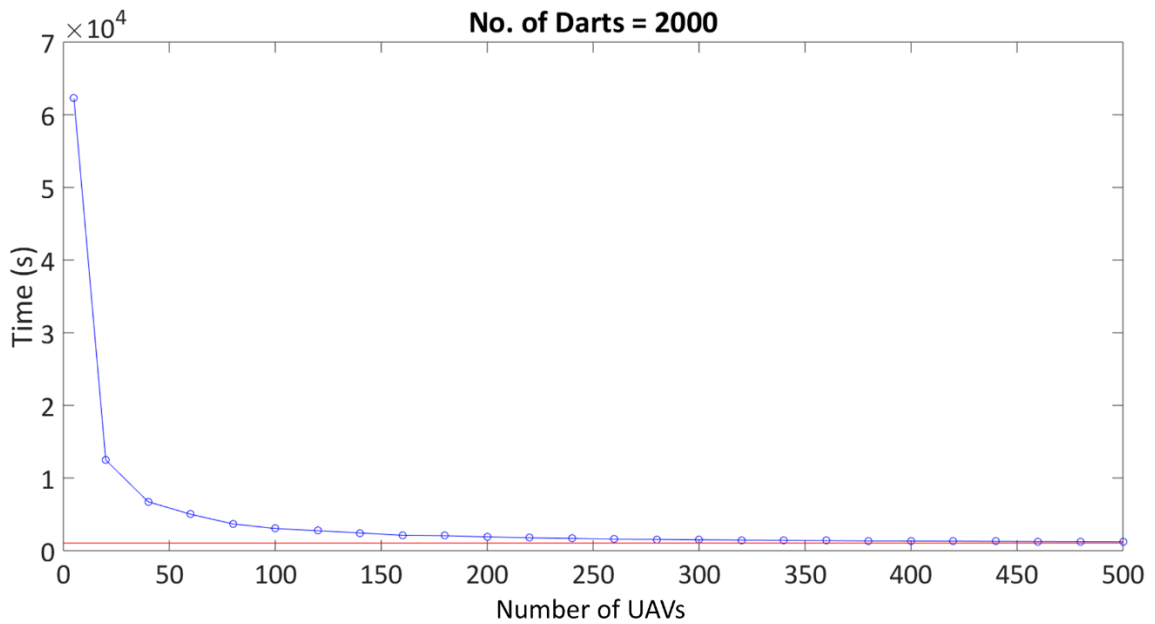


Fig. 38: Survey time for a 1km x 10 km region for different numbers of UAVs.

The Seismic UAV can deploy the SeismicSpider at a given waypoint. This attribute was not considered in the simulation but could be done to improve sensor deployment speed on SeismicSpiders. In Fig. 38 we vary the percentage of individual types of sensors but keep the total number of sensors a constant. The goal is to analyze ratios of different sensors to optimize cost and time. 10 SeismicDarts are provided for each UAV.

Increasing the percentage of UAVs lowers the deployment time. This is obvious since UAVs move at 20 m/s whereas SeismicSpiders move at 0.2 m/s. The difference in velocities makes UAV deployment time efficient. The SeismicSpiders are ideal for hard surface sensing or regions difficult for UAVs to access such as forests.

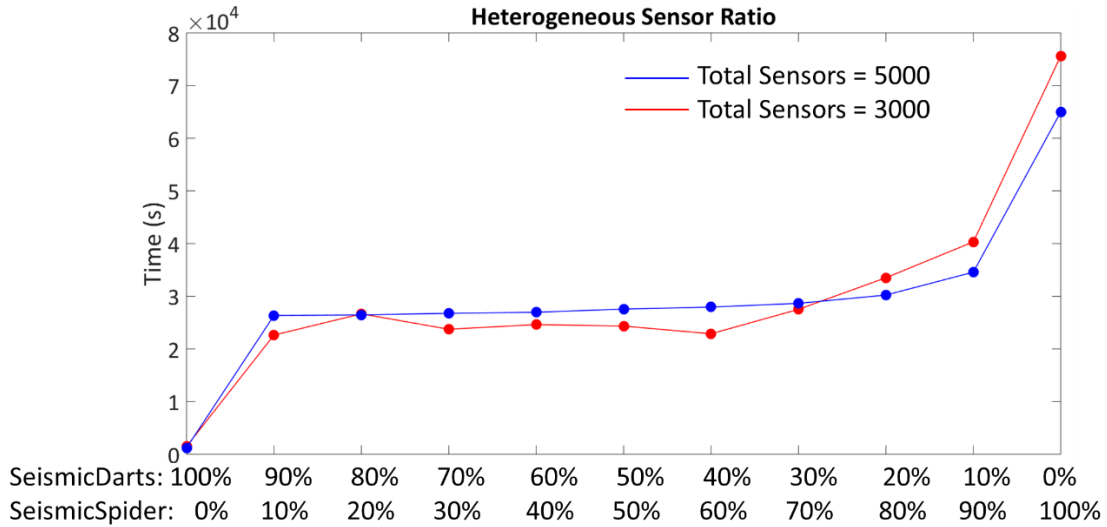


Fig. 39: Survey time for different sensor ratios. The total number of sensors {5000, 3000} were kept constant. Ten darts were provided for each UAV.

CHAPTER 5: CONCLUSION AND FUTURE WORK

This work presented an autonomous technique for geophone placement, recording, and retrieval. The system enables automating a job that currently requires large teams of manual laborers. Three components were introduced, SeismicDarts, a mobile SeismicSpider, and a deployment unit. Field and laboratory hardware experiments demonstrated the efficacy of the robotic team compared to traditional techniques. The SeismicDart's output was comparable to well-planted geophones, suggesting the feasibility of the proposed system. For hard surfaces where the SeismicDart could not penetrate, an autonomous alternative was presented, the SeismicSpider. The SeismicSpider is mobile, can actively adjust its sensors to ensure ground contact and vertical placement, and can be deployed and retrieved by UAVs. The autonomous deployment was conducted using GPS, proving human involvement could be drastically minimized by adopting the proposed technique. Hardware experiments compared the autonomous system to manual planting and ballistic deployment. Simulation studies show time and cost savings over traditional manual techniques.

An optimized path-planning algorithm was simulated for servicing a WSN. The path constructed is adaptive to the sensor node locations. The simulations above used a static WSN, but often sensor data transmission is dependent on transient phenomena. For example, a swarm of subsea sensors may track a school of fish, the progress of an oil slick, or seasonal drift of ocean currents. These are time-varying phenomena, and so the UAV servicing the sensors should be able to adapt. The same local optimization techniques presented in this work should be able to iteratively adapt the paths of UAVs.

Finally, future work should extend our simulation to handle non-stationary sensor nodes, improve the convergence rate, and use mTSP code to escape local minima. Future drone systems could be designed solely for seismic exploration purposes thereby increasing robustness, increasing flight and stationary periods, and could be weatherized. A new direction in this project would be to perform fast data transmissions between the different sensors (clients) and the UAVs (servers). The proposed algorithms and simulations could be implemented where the UAV would not only act as a deployment unit but will also hover above these sensors to collect data and (if possible) recharge their batteries. This research has innumerable application domains beyond seismic surveying. This added feature would help with faster analysis of the physical region. Another future direction would be to improve the GPS navigation system by adding visual servo control. This would enhance precision and also would aid in retrieving the sensors from the field. These features together will completely automate the process of seismic sensing, an important milestone in the geophysics community.

REFERENCES

- [1] International Energy Agency, “2014 Key World Energy Statistics,” pp. 6–38, May 2014. [Online]. Available: <http://www.iea.org/publications/freepublications/>
- [2] Victor Shnayder, Mark Hempstead, Bor rong Chen, Geoff Werner Allen, and Matt Welsh. *Simulating the Power Consumption of Large-Scale Sensor Network Applications*. ACM Sensys, Baltimore, MD, November 2004.
- [3] I.F. Akyildiz, W. Su, Y. Sankarasubramaniam, and E. Cayirci. *Wireless Sensor Networks: A Survey*. Elsevier Computer Networks Journal, 38(4):169–181, September 2002.
- [4] Y. T. Hou, Y. Shi, H. D. Sherali, and S. F. Midkiff. *On Energy Provisioning and Relay Node Placement for Wireless Sensor Networks*. IEEE Transactions on Wireless Communications, 4(5):2579–2590, September 2005.
- [5] T. Jian, H. Bin, and S. Arunabha. *Relay Node Placement in Large Scale Wireless Sensor Networks*. Computer Communications, 29(4):490–501, February 2006.
- [6] Y. Shi, L. Xie, Y. T. Hou, W. Lou, and H. D. Sherali. *On Renewable Sensor Networks with Wireless Energy Transfer: The Multi-node Case*. IEEE International Conference on Computer Communications, INFOCOM 2011, Shanghai, China, April 2011.
- [7] C. Hua and T. P. Yum. *Optimal Routing and Data Aggregation for Maximizing Lifetime of Wireless Sensor Networks*. IEEE/ACM Transactions on Networking, 16(4):892–903, August 2008.
- [8] The Green Cross and Blacksmith Institute. *The World’s Worst Pollution Problems 2012: Assessing Health Risks at Hazardous Waste Sites*. Blacksmith Institute, Zurich/New York, 2012.

- [9] Natural Resources Defense Council. “Proper Disposal of Batteries, Electronics and Hazardous Waste.”
- [10] Andr Kurs, Aristeidis Karalis, and Robert Moffat, *Wireless Power Transfer via Strongly Coupled Magnetic Resonances*. *Science*, 317(5843):83–86, June 2007.
- [11] Kai-Wei Fan, Zizhan Zheng, and Prasun Sinha. *Steady and Fair Rate Allocation for Rechargeable Sensors In Perpetual Sensor Networks*. ACM Conference on Embedded Network Sensor Systems, SenSys 2008, New York, NY, November 2008.
- [12] L. Xie, Y. Shi, and Y. Hou. *Making Sensor Networks Immortal: An Energy-Renewal Approach with Wireless Power Transfer*. *IEEE/ACM Transactions on Networking*, 20(6):1748–1761, December 2012.
- [13] Tolga Bektas. *The Multiple Traveling Salesman Problem: An Overview of Formulations and Solution Procedures*. *Omega*, 34(3):209–219, 2006.
- [14] G. B. Dantzig and J. H. Ramser. *The Truck Dispatching Problem*. *Management Science*, 6(1):80–91, 1959.
- [15] Stephen L Smith, Mac Schwager, and Daniela Rus. *Persistent Robotic Tasks: Monitoring and Sweeping in Changing Environments*. *IEEE Transactions on Robotics*, 28(2):410–426, 2012.
- [16] Daniel E Soltero, Mac Schwager, and Daniela Rus. *Decentralized Path Planning for Coverage Tasks Using Gradient Descent Adaptive Control*. *The International Journal of Robotics Research*, 2013.
- [17] Soroush Alamdari, Elaheh Fata, and Stephen L Smith. *Persistent Monitoring in Discrete Environments: Minimizing the Maximum Weighted Latency Between Observations*. *International Journal of Robotics Research*, 33(1):138–154, January 2014.

- [18] Zanjie Huang, Hiroki Nishiyama, Nei Kato, Fumie Ono, and Ryu Miura. *Resource Allocation for Data Gathering in UAV-Aided Wireless Sensor Networks*. IEEE International Conference on Network Infrastructure and Digital Content (IC-NIDC 2014), Beijing, China, September 2014.
- [19] Shimin Guo, Majid Ghaderi, Aaditeshwar Seth, and Srinivasan Keshav. “Opportunistic scheduling in ferry based networks,” 2006.
- [20] Shimin Guo and Srinivasan Keshav. “*Fair and Efficient Scheduling in Data Ferrying Networks*.” ACM CoNEXT Conference, CoNEXT-2007, pages 13:1–13:12, New York, NY, USA, 2007.
- [21] Kart A Swieringa, Clarence B Hanson, Johnhenri R Richardson, Jonathan D White, Zahid Hasan, Elizabeth Qian, and Anouck Girard. *Autonomous Battery Swapping System for Small-Scale Helicopters*. IEEE International Conference in Robotics and Automation (ICRA), 2010, pages 3335–3340. IEEE, 2010.
- [22] Tuna Toksoz, Joshua Redding, Matthew Michini, Bernard Michini, Jonathan P How, M Vavrina, and John Vian. *Automated Battery Swap and Recharge to Enable Persistent UAV Missions*.” AIAA Infotech at Aerospace Conference, 2011.
- [23] Yash Mulgaonkar. “Automated recharging for persistence missions with multiple micro aerial vehicles.” PhD thesis, University of Pennsylvania, 2012.
- [24] Brent Griffin and Carrick Detweiler. “*Resonant Wireless Power Transfer to Ground Sensors from a UAV*.” IEEE International Conference in Robotics and Automation (ICRA), 2012, pages 2660–2665. IEEE, 2012.
- [25] Jennifer Johnson, Elizabeth Basha, and Carrick Detweiler. *Charge Selection Algorithms for Maximizing Sensor Network Life With UAV-Based Limited Wireless*

Recharging. IEEE Eighth International Conference on Intelligent Sensors, Sensor Networks and Information Processing, 2013, pages 159–164. IEEE, 2013.

[26] Liguang Xie, Yi Shi, Y. Thomas Hou, and A. Lou. “Wireless power transfer and applications to sensor networks.” *Wireless Communications, IEEE*, 20(4):140–145, 2013.

[27] Neil Mathew, Stephen L Smith, and Steven Lake Waslander. “A Graph Based Approach to Multi-Robot rendezvous for Recharging in Persistent Tasks.” In IEEE International Conference on Robotics and Automation (ICRA), 2013, pages 3497–3502. IEEE, 2013.

[28] Esther M Arkin, Sándor P Fekete, and Joseph SB Mitchell. “Approximation Algorithms for Lawn Mowing and Milling.” *Computational Geometry*, 17(1):25–50, 2000.

[29] Aaron Becker. “Lloyd’s Algorithm.” MATLAB Central File Exchange, April 2013.

[30] Stuart Lloyd. “Least Squares Quantization in PCM.” *IEEE Transactions on Information Theory*, 28(2):129–137, 1982.

[31] Srikanth Kandanuru Venkata Sudarshan and Aaron T. Becker. “Decentralized Path Planning for Coverage using Gradient Descent Adaptive Control.” MATLAB Central File Exchange, February 2015.

[32] Fritz Peter Fischer. “U“ Ber Die Darstellung Der Hornhautoberfl“Che Und Ihrer Ver“Anderungen Im Reflexbild.” Springer, 1928.

[33] David Applegate, Robert Bixby, Vašek Chvátal, and William Cook. “Finding Tours in the TSP.” Citeseer, 1999.

[34] David Applegate, William Cook, Sanjeeb Dash, and André Rohe. Solution of a Min-Max Vehicle Routing Problem.” *INFORMS Journal on Computing*, 14(2):132–143, 2002.

- [35] Victor Shnayder, Mark Hempstead, Bor Rong Chen, Geoff Werner Allen, and Matt Welsh. Simulating the Power Consumption of Large-Scale Sensor Network Applications. in ACM Sensys, Baltimore, MD, November 2004.
- [36] Joseph Kirk. “Fixed Start/End Point Multiple Traveling Salesmen Problem- Genetic Algorithm” (MATLAB code), May 2014.
- [37] P. M. Shearer, Introduction to Seismology. Cambridge University Press, 2009.
- [38] G. W. Wood, R. L. Workman, and M. W. Norris, “Distributed Seismic Data-Gathering System,” Mar. 3 1998, US Patent 5,724,241.
- [39] J. Jiang, A. A. Aziz, Y. Liu, and K.-M. Strack, “Geophysical Data Acquisition System,” Jun. 16 2015, US Patent 9,057,801.
- [40] Goins, Neal Rodney, A. M. Dainty, and M. N. Toksöz, “*Lunar Seismology: The Internal Structure of the Moon.*” in Journal of Geophysical Research: Solid Earth 86.B6, 1981, pp. 5061–5074.
- [41] Jean-Jacques Postel, Thomas Bianchi, Jonathan Grimsdale, “Patent US20140307525: Drone Seismic Sensing Method and Apparatus,” October 2014. [Online]. Available: <https://www.google.com/patents/US20140307525>
- [42] Mars Advanced Planning Group 2006, “Robotic Mars Exploration Strategy 2007–2016,” March 2006. [Online]. Available: https://mepag.jpl.nasa.gov/reports/3715_Mars_Expl_Strat_GPO.pdf
- [43] Srikanth. K. V. Sudarshan, L. Huang, C. Li, R. Stewart, and A. T. Becker, *Seismic Surveying with Drone-Mounted Geophones*, in CASE, 12th Conference on Automation Science and Engineering. IEEE, 2016, pp. 1–6.

- [44] Vicor. B. Montano and A. T. Becker, “SeismicDart,” Sep. 2016. [Online]. Available: <http://www.thingiverse.com/thing:1713499>
- [45] T. Miyazaki, K. Mukaiyama, Y. Komori, K. Okawa, S. Taguchi, and H. Sugiura, *Aerodynamic Properties of an Archery Arrow*, Sports Engineering, vol. 16, no. 1, pp. 43–54, 2013.
- [46] Srikanth. K. V. Sudarshan and Aaron T. Becker, “Seismic Survey Scheduler.” MATLAB Central File Exchange, Sep. 2016. [Online]. Available: <http://www.mathworks.com/matlabcentral/fileexchange/59034>